Photochemical aging of aerosol particles in different air masses arriving at Baengnyeong Island, Korea

Eunha Kang[1,5], Meehye Lee[1]*, William H. Brune[2], Taehyoung Lee[3], Taehyun Park[3], Joonyoung Ahn[4], Xiaona Shang[1]

[1]Department of Earth and Environmental Sciences, Korea University, Republic of Korea

[2]Department of Meteorology, Pennsylvania State University, USA

[3]Department of Environmental sciences, Hankuk University of Foreign Studies, Republic of Korea

[4]National Institute of Environmental Research, Republic of Korea

[5]Department of Urban and Environmental studies, Suwon Research Institute, Republic of Korea

Submitted to Atmospheric Chemistry & Physics

December 2016

[1*] Corresponding author, meehye@korea.ac.kr

Abstract

Atmospheric aerosol particles are a serious health risk, especially in regions like East Asia. We investigated the photochemical aging of ambient aerosols using a potential aerosol mass (PAM) reactor at Baengnyeong Island in the Yellow Sea during August 4–12, 2011. The size distributions and chemical compositions of aerosol particles were measured alternately every 6 min from the ambient air or through the highly oxidizing environment of a Potential Aerosol Mass (PAM) reactor. Particle size and chemical composition were measured by the combination of a Scanning Mobility Particle Sizer (SMPS) and a High Resolution-Time of Flight-Aerosol Mass Spectrometer (HR-ToF-AMS). Inside the PAM reactor, O_3 and OH levels were equivalent to 4.6 days of integrated OH exposure at typical atmospheric conditions. Two types of air masses were distinguished on the basis of the chemical composition and the degree of aging: air transported from China, which was more aged with higher sulfate concentration and O:C ratio; and the air transported across the Korean Peninsula, which was less aged with more organics than sulfate and lower O:C ratio. For both episodes, the particulate sulfate mass concentration increased in the 200–400 nm size range when sampled through the PAM reactor. A decrease in organics was responsible for the loss of mass concentration in 100–200 nm particles when sampled through the PAM reactor for the organic-dominated episode. This loss was especially evident for the *m/z* 43 component, which represents. The *m/z* 44 component, which represents further oxidized organics increased with a shift toward larger sizes for both episodes. It is not possible to quantify the maximum possible organic mass concentration for either episode because only one OH exposure of 4.6 days was used, but it is clear that SO_2 was a primary precursor of secondary aerosol in northeast Asia especially during the long-range transport from China. In addition, inorganic nitrate evaporated in the PAM reactor as sulfate was added to the particles. These results suggest that the chemical composition of aerosols and their degree of photochemical aging particularly for organics, are also crucial in determining aerosol mass concentrations.

1. Introduction

In East Asia, atmospheric aerosols are a cause of public concern because of the frequent occurrence of haze in mega cities and industrial areas, dust storms in deserts and extremely dry regions, and their transboundary transport (Takami et al., 2007; Wu et al., 2009; Kim et al., 2009; Ramana et al., 2010; Kang et al., 2013). These occurrences impact the regional air quality and climate (Li et al., 2011; Huang et al., 2014). Aerosol plumes are able to remain in the atmosphere for up to 10 days and can be transported across the Pacific Ocean. During transport, air masses become photochemically aged, leading to the generation of secondary aerosols and subsequent modification of the optical and microphysical properties of aerosols (Dunlea et al., 2009; Lim et al., 2014; Lee et al., 2015). This transformation process has been studied by collecting ambient air across the Pacific Ocean or by tracking the Asian plumes onboard aircraft (Brock et al., 2004; Aggarwal and Kawamura, 2009; Dunlea et al., 2009; Peltier et al., 2008).

Secondary aerosols comprise inorganics such as sulfate and nitrate as well as organics. Of these, secondary organic aerosols (SOA) are of more interest because they are produced in the atmosphere from numerous organic species and are aged through complex mechanisms, during which their physicochemical properties such as volatility, hygroscopicity, and optical properties are altered. The absorption and scattering properties of aerosols in northeast Asia was reported to be intimately linked with their chemical composition (Lim et al., 2014). As aerosols are oxidized, the hygroscopicity of organic aerosols (OAs) increases, suggesting photochemically driven CCN activation of SOA (Massoli et al., 2010; Lambe et al., 2011; King et al., 2010; Morgan et al., 2010).

To understand SOA formation and aging processes, experiments have been conducted using environmental chambers (Kroll and Seinfeld, 2008; Hallquist et al., 2009). In these large environmental chambers, atmospheric simulations are limited to the equivalent of only about a day, which is much shorter than the nominal atmospheric lifetime of aerosols, which is about a week. In addition, ambient air masses are under

influence of various emissions and mixing processes, which are not properly represented in these well-mixed and long-residence time chambers (Jimenez et al., 2009; Ng et al., 2010).

Thus, we introduced the potential aerosol mass (PAM) chamber, a continuous flow reactor under high levels of OH and O_3, which is applicable for both controlled lab studies and ambient air (Cubison et al., 2011; Kang et al., 2007, 2011b; Lambe et al., 2012; Massoli et al., 2010). The highly oxidizing conditions of the PAM reactor are suitable for examining SOA formation and oxidation processes for the equivalent of a week or more (Jimenez et al., 2009; George and Abbatt, 2010). In particular, the PAM reactor has less wall loss mainly due to much shorter residence time compared to conventional chambers. Thus, PAM reactor is able to reasonably simulate aging processes of SOA after formation (Kang et al., 2011a). In the first field deployment of PAM in northeast Asia, Kang et al. (2011a) reported PAM simulation results for different air masses and demonstrated that oxidation processes occurring in the natural atmosphere were plausibly integrated in the PAM reactor. Recently, PAM reactor has been used to examine secondary aerosol formation and evolution from ambient air masses (Hu et al., 2016; Ortega et al., 2016; Palm et al., 2016) and emission sources (Ortega et al., 2013; Link et al., 2017; Timonen et al., 2017). The wall losses of aerosols and condensable gases and photochemistry of the PAM reactors have been studied to quantitatively understand the experimental results of PAM reactor (Lamb et al., 2015; Palm et al., 2016; 2017; Peng et al., 2015; 2016).

In this study, we deployed a PAM reactor at an island site in the Yellow Sea to investigate the photochemical aging of ambient aerosols in sulfate-dominated northeast Asia. The particle size, mass and chemical characteristics of ambient and PAM-processed aerosols were compared for different air masses transported from nearby continents. Their aging characteristics were examined in terms of secondary aerosol formation and evolution of pre-existing aerosol particles. The discussion mainly focused on the formation of sulfate and further oxidized organics and the loss of less oxidized organics upon photochemical oxidation in PAM reactor.

2. Experimental methods

Experiments were conducted at a measurement station on Baengnyeong Island in the Yellow Sea (37.967°N, 124.630°E, 100 m asl) from August 4 to August 12, 2011 (Fig. 1a). As the northernmost and westernmost part of South Korea, Baengnyeong Island is located 740 km west of Beijing and 211 km east of Seoul. The measurement station was established by the National Institute of Environmental Research (NIER) as a core background site of the National Monitoring Network to observe dust and pollution plume transported from China. In previous studies conducted at the same site, sulfate and organic aerosols were enhanced under the influence of pollution plumes transported from eastern China and the Korean Peninsula (Choi et al., 2016; Lee et al., 2015).

Ambient air sampled using a $PM_{2.5}$ cyclone was pulled through a tubing (1 cm diameter) into the PAM reactor for 6 minutes, during which time the ambient aerosols were oxidized (hereafter referred to as "PAM aerosols"). For another 6 minutes, the sampled ambient air was directly pumped into the analytical instruments, bypassing the PAM reactor. The ambient and PAM aerosols were alternately measured every 6 minutes, thereby producing pseudo-simultaneous measurements.

The PAM reactor employed in this study is the same version as that described in Lambe et al. (2011), which was also used for laboratory studies of SOA aging (Lambe et al. 2012; 2015) (S1). The ambient air was introduced into the PAM reactor through a Silconert-coated (Silcotech, Inc.) inlet plate and endcap and then rapidly dispersed before entering the reactor through a Silconert-coated stainless-steel screen. For aerosol sampling, copper or stainless steel 1/4 inch OD tubes were used to minimize the particle loss on the tubing walls. The 1/4 inch PTFE Teflon tubes were used for the bypass flow. The total flow rate through the both ambient sampling and PAM reactor was 5 liters per minute. The flow in the PAM reactor was laminar (Reynolds number <50), and aerosols were sampled at the center line. The residence time of air in the PAM reactor was 100 seconds based on flow rate and the volume of the reactor. During the experiment, the loss

129 associated with PAM reactor and inlet was determined. The SO_2 loss through a cyclone
130 and inlet plate was 11 ± 7 % and aerosol particle loss in the PAM reactor was about 12 %
131 (Figure S2-1; S2-2). The loss of particles and SO_2 gas was measured as difference in the
132 concentration between ambient air and air pulled through PAM reactor with UV lights off.
133 In addition, the three-way switching valve might cause the evaporation of ambient and
134 PAM aerosols when it was getting hot during operation.
135 The PAM reactor is equipped with 30-cm long Hg lamps emitting 185 nm and
136 254 nm light (82-9304-03, BHK Inc.) in order to produce large amounts of OH and O_3,
137 creating a highly oxidizing environment (Figure S1). The UV lamps were housed in Teflon
138 sleeves being purged by nitrogen with a flow rate of ~50 sccm to prevent O_3 from
139 building up inside the sleeves. This flow also slightly lowers the amount of heat being
140 transferred from the lamps to the air in the chamber. The results of Ortega et al. (2016)
141 using the PAM reactor same as that used in the present study, demonstrated that
142 temperature increased by about 2 ℃ inside the PAM reactor. In a recent discussion, a
143 10 ℃ difference between PAM and ambient air caused the evaporation of inorganic nitrate
144 up to 34 % and OA up to 25 % (2016-10-17_PAM_Users_Mtg_Jimenez_Group_Final_v2.pdf).
145 However, the ambient temperatures were 20~26℃ which equaled or exceeded the
146 temperature of the air-conditioned laboratory, which was set to 20℃. As a result, the
147 temperature difference between the PAM reactor and the ambient air was at most a few
148 degrees. Thus, temperature-induced evaporation of OA or nitrate in the PAM reactor
149 would likely have been small.
150 In this study, the OH exposure of the PAM reactor was dependent on the
151 humidity of the ambient air but not modulated by UV lamps. The exposure was originally
152 set to 3-4 days for spring time to get near-maximum mass concentration. However, the
153 experiment was delayed by logistic problem and the OH exposure was closer to 4.6 days
154 due to high humidity in summer.
155 The OH exposure of PAM reactor was estimated to be 7 x 10^{11} molecules cm^{-3} s
156 against sulfur dioxide decay that was conducted by Kang et al., 2011b (Figure S3-1.). When

157 corrected for calculated OH suppression, it was 25% lower than from the SO_2 calibration
158 and was equivalent to an integrated OH concentration over 4.6 days at a typical noon-
159 time concentration of 1.5 x 10^6 molecules cm^{-3} (Mao et al., 2010). The OH suppression
160 from VOCs and other OH-reactive gases were calculated using the oxidation chemistry
161 model (Peng et al., 2016) with 30 s^{-1} of external OH reactivity, representing rural areas
162 (Feiner et al., 2016; Lee et al., 2008; Peng et al., 2016; Yoshino et al., 2006). Using this OH
163 exposure, the calculated sulfate production matches the measured sulfate increase in the
164 PAM reactor to within 16 % (Figure S4-1).

165 The chemical composition of the aerosol particles was measured by a high-
166 resolution time-of-flight aerosol mass spectrometer (HR-ToF-AMS, hereafter referred to as
167 "AMS"). The number concentration was determined in the mobility diameter range of
168 10.4–469.8 nm with a scanning mobility particle sizer (SMPS 3034, TSI) (Jayne et al., 2000;
169 Jimenez et al., 2003; DeCarlo et al., 2006; Drewnick et al., 2006). Detailed descriptions of
170 the HR-ToF-AMS and the sampling site can be found elsewhere (Lee et al., 2015). For AMS
171 measurements, a composition-dependent collection efficiency was applied by adopting the
172 result of Middlebrook et al. (2012). Due to the detection range of the SMPS, the
173 enhancement or loss of particles greater than 500 nm in diameter were not observed in
174 SMPS measurement. The particle mass concentration from SMPS was obtained from the
175 volume concentration multiplied by a fixed particle density of 1.4 g cm^{-3}.

176 Some of the condensable gases formed in the PAM reactor do not contribute to
177 the observed particle mass concentration sampled by the SMPS and AMS at the exit of the
178 PAM reactor. Some are deposited on the PAM reactor walls, and some do not condense
179 before the particles are sampled. The calculation of the condensation sink indicates the
180 fraction that are measured as particles. These calculations indicate that typically 60 % to
181 70 % of the condensable gases did condense on particles before the particles were
182 measured (Figure S5). The particle mass concentrations shown in the results have been
183 corrected for this loss and the details of the correction is described in supplemental
184 information (S6). The resulting mass concentrations sampled through the PAM reactor and

sampling system have an uncertainty of ±20 % (2σ confidence).

The overall mass spectra of organics indicate substantial loss of less oxidized OAs (e.g., *m/z* 41, 42, 43, ...) in the PAM reactor. In addition, CO^+ and CO_2^+ groups increased and decreased in the PAM aerosol particles during these measurements. The terms *m/z* 43 and *m/z* 44 from the mass spectra correlate with less oxidized OAs and further oxidized organics such as carboxylic acids, respectively. Therefore, the discussion of ions observed at *m/z* 43 and *m/z* 44 should be broadly applicable to these two classes of organic compounds.

Gas-phase ozone (O_3), nitrogen dioxide (NO_2), carbon monoxide (CO), and particle-phase elemental carbon (EC) and organic carbon (OC) were simultaneously measured, along with meteorological parameters (Table 1). The HYSPLIT backward trajectory model, which was developed by the National Oceanic and Atmospheric Administration (NOAA), was used to examine the history of the sampled air masses (Wang et al., 2009).

In thist study, therefore, we examined how the air masses reaching Baengnyeong Island were further oxidized during the effective aging time of 4.6 days, which is consistent with transport time from China but slightly longer than the time of typical maximum SOA production from aging (Ortega et al., 2016) under an OH diel-mean of 1.5 x 10^6 molecules cm^{-3}.

3. Results

3.1. Measurement overview of ambient and PAM aerosols

$PM_{1.0}$ aerosol particle mass concentrations varied from 0.5 to 44 μg m^{-3} for both the PAM aerosol particles and the ambient aerosol particles (Figure 2(a)) during the entire experiment period. Choi et al. (2016) reported the AMS measurements ($PM_{1.0}$) made at the same site during March-April, 2012 and November-December, 2013, where $PM_{1.0}$ varied from the detection limit to ~100 μg m^{-3}. These $PM_{1.0}$ concentrations were lower than those

measured in Changdao that is located in Bohai Sea (Hu et al., 2013; Choi et al., 2016; Lee et al., 2015). The PAM particle mass concentration was generally greater than the ambient particle mass concentration.

Particle mass concentration distributions of the ambient and PAM aerosol particles were averaged for the entire experiment and their difference is presented in Fig. 3. In the PAM reactor, the formation of nucleation mode particles were always observed (average dN/dlogDp = 2 x 10^5 cm^{-3}, see Figure S9), but their contribution to the total particle mass concentration was relatively insignificant due to their small sizes of less than 50 nm in diameter (Dp). In comparison, the mass concentration of PAM aerosol particles increased at sizes larger than 200 nm. The averaged particle mass concentration between 50 and 200 nm in diameter was enhanced in PAM reactor for the sampling period (Fig 3), but in detail, particles were either lost or produced in the PAM reactor, depending on the history of the air masses (Figures 5 and Figure S9). The formation of nucleation mode particles in PAM reactor were also observed in previous studies (Kang et al., 2011b; Ortega et al., 2016; Palm et al., 2016). Major constituents including sulfate, organics, ammonium, and nitrate for both ambient and PAM particles are presented in Fig 3. Sulfate and ammonium concentrations in the PAM reactor were mostly higher or similar to those in the ambient air. In contrast, total organics and nitrate were mostly lower in the PAM aerosol particles than in ambient aerosol particles.

Previous studies show that the SOA formation from VOCs including Semi/Intermediate Volatile Compounds (S/IVOCs) near the sources could be enhanced up to a few times greater than SOAs from VOCs only (Hayes et al., 2015; Palm et al., 2016). It is possible that S/IVOCs could be lost to the reactor inlet plate as well as reactor wall due to their low saturation vapor pressures, leading to the underestimation of their contribution to SOA formation in the PAM reactor of this study. However, in our experiment, air masses had traveled at least a day from the Korean Peninsula or from east China before they were sampled in the PAM reactor. Thus, it is likely that S/IVOCs were already partitioned into the particle phase before the particles were sampled at the

241 measurement station on Baengnyeong Island.

242

243 **3.2. Organics- and sulfate-dominated episodes**

244

245 Throughout the study, ambient aerosol particles were enhanced during two
246 separate periods (shaded in Fig. 2a), with distinct differences in chemical composition
247 between the two. While the ambient air was enriched in organics during the first episode
248 (August 6, 11 AM to August 7, 9 AM), sulfate was dominant in the second episode (August
249 9, 1 AM to August 9, 6 PM). During the two episodes, the levels of gaseous precursors
250 including NOx, SO_2, and CO were higher than in the remaining periods (Fig. 4). The ratios
251 of both SO_2/NOx and OC/EC were higher and the ratio of O_3/CO was lower for the first
252 case.

253 These two cases were distinguished by the air-mass backward trajectories (Fig. 1b).
254 Air passing over the Korean Peninsula had higher concentrations of organics than sulfate
255 during the first episode. For the second episode, the air mass backward trajectory
256 indicates that the sulfate–dominated air had been transported from southeast China. In
257 addition, the air mass trajectories imply that sulfate-dominated aerosols lingered over the
258 Yellow Sea and were aged more than the organic-dominated aerosols.

259 In addition, the aerosol particles differed in terms of size distributions between the
260 two episodes (Fig. 5 and Table 1). In the PAM reactor, the particle mass concentration
261 increased for particles smaller than 50 nm and larger than 200 nm increased for both
262 episodes. At size between 50 and 200 nm, however, the mass concentration of PAM-
263 processed particles increased during sulfate-dominated episode but slightly decreased
264 during organic-dominated episode.

265 The difference between AMS measured particle mass concentration and SMPS
266 measured particle mass concentration was greater in sulfate-dominated episodes than in
267 organic-dominated episode (Table 1 and Fig. 2(c)). The disagreement is largely associated
268 with AMS and SMPS measurement uncertainties. However, the role of elemental carbon or

soil particles that are abundant in the study region (Lee et al., 2007; Lim et al., 2012) may not be ruled out because there are captured by SMPS but not by AMS.

The measurement results of size-separated chemical compositions provide detailed information on transformation processes in the PAM reactor. In general, aerosol particles in the PAM reactor experienced an increase in sulfate but a decrease in total organics and nitrate compared to the ambient aerosol particles (Fig. 6). The enhancement of sulfate in PAM reactor was greater for sulfate-dominated episode, and the reduction of organics in PAM reactor was greater for organic-dominated episode. The contribution of ammonium ions to the total mass concentration was also greatest when aerosol particles were enriched in sulfate. The *m/z* 43 decreased and *m/z* 44 increased in the PAM reactor for both episodes. (Fig. 5).

Therefore, the following discussion is focused on these two distinct aerosols episodes. The size-separated chemical compositions are thoroughly examined and compared in order to elaborate on the formation of secondary aerosols and the evolution of ambient aerosols upon photo-oxidation in the PAM reactor.

4. Discussion

4.1. Nucleation of particles

In the current study, freshly nucleated particles (Dp <50 nm) were always observed in the PAM reactor (Figure 2(d)). In both cases, there was sufficient SO_2 and likely ammonia to nucleate new particles, but nucleation by extremely low-volatility organics cannot be ruled out. In previous field studies, increases in the mass concentration of PAM aerosol particles were dependent on the ambient SO_2 concentrations (Kang et al., 2013). Palm et al. (2016) also observed the nucleation mode particles formed, competing for the role of condensation sink with pre-existing accumulation mode particles. The number concentrations of nucleation-mode particles in PAM reactor in the organic-dominated episode was an order of magnitude greater than them in the sulfate-dominated episode

while the SO_2 mixing ratios were similar (details in Figure S9). This could be evidence for nucleation of the extremely low volatility organic compounds called Highly Oxygenated Molecules (HOMs) (Tröstl et al., 2016). Chemical composition was not available for nucleation mode particles due to an AMS cut-off size of 50 nm in the present study. VOC concentrations for ambient air were not determined either.

4.2. Formation and evolution of organic aerosols

The SMPS mass size distributions highlight the size range of 100~200 nm, where PAM particle mass concentration was reduced for organic-dominated episode (Fig. 5). A previous study showed that the less oxidized organic aerosols were found more often than more oxidized OAs in particles smaller than 200 nm (Sun et al., 2012). In addition, the mass concentration of *m/z* 43 was higher in less oxidized OAs than more oxidized OAs (Sun et al., 2012). In the present study, the contribution of *m/z* 43 to total organics was greater in the organics-dominated episode than in the sulfate-dominated episode, and the loss of organics in PAM reactor was also greater in the organics-dominated episode. These results suggest that the less oxidized OAs were more in the organics-dominated episode than in the sulfate-dominated episode. The ratios of O:C were lower for organic-dominated aerosol particles than those of sulfate-dominated aerosol particles (Fig. 7). These results for the particle composition are consistent with the air mass trajectories (Fig. 1b), which show that the organic-dominated air masses were relatively less aged than those of the sulfate-dominated episode (Jimenez et al., 2009; Ng et al., 2011).

The AMS measurement results indicate that total organics and the *m/z* 43 component were consistently reduced in the PAM reactor. Possible loss mechanisms are the deposition of aerosol particles on the chamber wall (McMurry and Grosjean, 1985; La et al., 2016) and fragmentation reactions from further photo-oxidation to form products with higher vapor pressure (Lambe et al., 2012). As described in the section 3, the condensable organics loss by wall surface and by heterogeneous oxidation were calculated to be about 30~40%. Also, mass concentration loss due to temperature differences in the

ambient air and in the PAM reactor are estimated to be minimal. For the entire experiment, the O:C ratios of PAM aerosol particles were greater than those of ambient aerosols, with O:C ratios corresponding to less oxidized OAs and more oxidized OAs (Zhu et al., 2018). Thus, a chemical transformation from low O:C to high O:C probably explains the organic mass loss.

Organics are known to be oxidized by OH undergoing functionalization and fragmentation. The pathway by which this occurs is determined by the oxidation state of the existing organic aerosol particles. Functionalization dominates in the early stage of oxidation, which increases total organics and *m/z* 43, while fragmentation dominates in the later stage of oxidation, reducing OA mass concentration (Jimenez et al., 2009; Kroll et al., 2009; Chacon-Madrid et al., 2010; Henry and Donahue, 2012; Lambe et al., 2012). For highly oxidized OAs with O:C ratios greater than 0.4, fragmentation becomes especially dominant, resulting in OA mass concentration loss.

In this study, the measured O:C ratios of the ambient aerosol particles were greater than 0.4 for both episodes (Fig. 7), which indicates that the observed ambient organic aerosol particles were aged enough to be fragmented. Figure 7 also shows that PAM OAs have higher O:C ratio and lower H:C ratio than ambient aerosol particles do and that the Van Krevelen slope (Δ(H:C)/ Δ(O:C)) of both episodes were about -0.6. In a laboratory PAM experiment, Lambe et al. (2012) observed a similar tendency and explained that as SOA oxidized, the Van Krevelen slope changed from minor fragmentation of carbonyl and acids/alcohol to major fragmentation of acids. In addition, Hu et al. (2016) demonstrated that fragmentation became an important pathway of OAs oxidation at OH exposure greater than 10^{11} molecules cm^{-3} s. At OH exposure of 7 x 10^{11} molecules cm^{-3} s, they observed 20 % of OA mass concentration loss by volatilization followed by fragmentation of heterogeneous reaction products on the particles. In the present study, the OH-induced OA mass concentration loss in PAM reactor was about 25 % and 28 % for organic-dominated and sulfate-dominated episode, respectively at our OH exposure of 7 x 10^{11} molecules cm^{-3} s (Table 1).

353 The *m/z* 44 mass concentration increased in PAM aerosol particles. In particular,
354 the increase in *m/z* 44 mass concentration was associated with larger sizes than the *m/z*
355 43 mass concentration loss (Fig. 6). As mentioned above, *m/z* 43 mass concentration loss
356 was significant for sizes less than 200 nm in AMS measurement, but most of the increase
357 in *m/z* 44 mass was concentration observed in the size greater than 200 nm. If particles
358 grew in size by heterogeneous oxidation of carbonyls to carboxylic acids on pre-existing
359 particle surfaces, the mass concentration decrease in *m/z* 43 should also have been
360 associated with an increase in the *m/z* 44 mass concentration by the addition of oxygen.
361 For both episodes, *m/z* 43 reduction was associated with *m/z* 44 enhancement in PAM
362 reactor, however the total organics mass concentration was decreased. This result implies
363 that the observed loss of particle mass concentration was caused by heterogeneous
364 oxidation, which resulted in fragmentation and evaporation. The oxidation of organics in
365 the atmosphere can occur both in the gas phase and through heterogeneous reactions.
366 The gas-phase reaction is tens of times faster than the heterogeneous reaction, being
367 limited by diffusion to the particle surface (Lambe et al., 2012). In our experiment, it was
368 not feasible to distinguish gas-phase oxidation of semi-volatile organics in equilibrium
369 with the particle phase from heterogeneous oxidation of organics on the particle surface.
370 The distributions of less oxidized organics such as carbonyl groups with a semi-volatile
371 nature in gaseous and particulate phases are controlled by the partitioning equilibrium
372 between the two phases. In contrast, further oxidized organics such as organic acid
373 groups with low volatility tend to preferentially remain in the particle phase (Ng et al.,
374 2011). It is, therefore, quite likely that the gas-phase concentration of *m/z* 43-like
375 compounds decreased by further oxidation in the PAM reactor, leading to evaporation of
376 organic *m/z* 43 in particle phase to be re-equilibrated with the decreased concentration in
377 gas phase. On the other hand, *m/z* 44-like compounds were sufficiently less volatile, thus
378 they underwent little evaporation to the gas phase. During the ~100 s of the residence
379 time in the PAM reactor, the gas-phase reactions would be more efficient than relatively
380 slower heterogeneous oxidation, but as the semi-volatile SOA compounds are depleted,

then heterogeneous oxidation becomes more important(Lambe et al., 2012).

It was also found in a previous study that the loss of OA mass concentration was less for highly oxidized OAs than for less oxidized OAs due to heterogeneous oxidation (Kessler et al., 2012). In addition to the loss of less oxidized organics (*m/z* 43), the AMS measurements indicated that highly oxidized OAs (*m/z* 44) were produced in the PAM reactor. In particular, the *m/z* 44 peak was found to occur in the same size range as that of sulfate. These results suggest that SOAs formed by gas-phase oxidation and subsequent condensation on the surface of existing sulfate particles. Indeed, robust evidence for this can be found in detailed laboratory studies of SOA formation on acidic seed particles (Jang et al., 2002; Jang et al., 2006; Kang et al., 2007).

This difference in behavior between the two episodes is consistent with the evolution of particle aging. The organic-dominated episode had particles that have been aged less and therefore contain less oxygenated molecules that can be further oxidized. The sulfate-dominated episode had more aged particles that were more depleted in semi-volatile organics so that further oxidation would need to proceed through heterogeneous oxidation even though it is slower than gas-phase oxidation.

4.3. Formation and evolution of inorganic aerosols

In the PAM aerosol particles, sulfate concentrations were always greater than or similar to those of the ambient aerosol particles for the entire experiment period. This increase is expected because ambient SO_2 was about 3 ppbv in both episodes and some of this SO_2 would be converted to sulfate and either nucleate or be deposited on existing particles in the PAM reactor (Kang et al., 2007). For the two selected episodes, sulfate mass concentration noticeably increased in accumulation mode (Figure 6). Although nucleation mode particles increased in number concentration to a great extent, their mass concentration contribution was small at the ambient level of gaseous precursors. In this study, the variation in ammonium concentrations was similar to that of sulfate (Fig. 2b). In

addition, the equivalent ratios of sulfate and nitrate to ammonium indicated that the ambient particles were mostly acidic.

In the organic-dominated episode, the increase of the PAM aerosol particles mass concentration for particles larger than 200 nm resulted from the formation of sulfate and *m/z* 44 as described earlier (Figs. 5, 6), in which sulfate exhibited a broad peak in 200–500 nm particles, as in ambient particles. In comparison, the sulfate increase shifted toward smaller sizes in 200–400 nm range during the sulfate-dominant episode, leading to a sharp peak at 200 nm. An increase in sulfate mass concentration was noticeable between 200–400 nm. A major inorganic constituent, nitrate, was lost in the PAM reactor during both episodes, with an ambient nitrate concentration that was comparable to the levels of sulfate and organics concentration (Fig. 2b). The nitrate concentration loss occurs in the PAM reactor because of the efficient conversion of SO_2 to sulfate, causing the particles to become acidic and causing particulate nitrate (HNO_3(p)) to evaporate. A plausible source of HNO_3(p) in the PAM reactor is the formation of gaseous HNO_3(g) and deposition on the particles. If a particle is acidic in the presence of sulfuric acids, nitrate easily evaporates back to the gas phase. As stated in section 2, the loss of nitrate by temperature-induced evaporation would be insignificant.

In organic-dominated episode, the normality balance of ammonium with sulfate and nitrate (sulfate + nitrate) [μeq/L] / ammonium [μeq/L] was 1.34 in ambient particles, which was reduced to 1.22 in PAM particles with enhanced sulfate and ammonium but with nitrate being lost (details in Figure S8). In the sulfate-dominated episode, the ammonium balance remained unchanged in PAM particles due to an equivalent loss of nitrate over the condensation mode with its mode being shifted toward larger size. These results illustrate the role of sulfate in determining chemical compositions and mass loadings of aerosol particles in northeast Asia.

4.4. Atmospheric implications

The ambient OAs in the present study were moderately to well-aged, as indicated by their O:C ratios being greater than 0.4. They were chemically and physically transformed in the PAM reactor, resulting in increased O:C ratios and decreased OA mass concentrations by photochemical oxidation and fragmentation processes. Although the oxidant levels of OH and O_3 in the PAM reactor far exceeded the ambient levels, the H:C and O:C ratios of the ambient and PAM OAs were in close agreement with those observed in the atmosphere (Ng et al., 2011) (Fig 7). These results provide good evidence for the ability of the PAM reactor to accelerate oxidation processes in ambient air under high O_3 and OH conditions and to represent atmospheric aging of approximately 5 days without physical removal processes such as dry/wet deposition. It further confirms that the PAM reactor is applicable for field studies to observe aging processes of various types of precursors and aerosols including emission sources and long-range transported air masses.

The O:C ratios of OAs from this study were plotted against aging time and compared with those observed in east Asia (Fig. 8), where the O:C ratios were found to increase with transport time across the Pacific Ocean (Takegawa et al., 2006; Takami et al., 2007; Dunlea et al., 2009). The O:C ratios of the bulk OAs depend on the mass concentrations of organic constituents because the saturation vapor pressure varies with the molecular weight of the organics (Donahue et al., 2006). Thus, the O:C ratios from different studies are not directly comparable if their OA concentrations vary over a wide range. In Figure 8, OA mass concentrations ranged up to 10 μg m^3 and thus a comparison among different sets of measurements is suitable. In the real atmosphere, the fate and evolution of secondary aerosols could be affected by scavenging of oxidized OAs and inorganic aerosols on the cloud droplets by aqueous aerosol surface reaction (Dunlea et al., 2009), nucleation of new particles due to the entrainment of free tropospheric air (Song et al., 2010), or dry deposition on the dust particles (Dunlea at al., 2009). It is noteworthy that the increase in O:C ratios with photochemical aging was slightly higher in our results than in those of previous studies, which is possibly due to the omission of

464 these scavenging processes in PAM reactor.

465 The results of this study imply that SO_2 plays a key role in increasing secondary
466 aerosol concentrations in east Asia because the lifetime of SO_2 is longer than those of
467 VOCs and because sulfate is relatively stable in the particle phase once formed, contrary to
468 nitrate and organics. While SOA formation is more important near sources or in fresh air
469 masses, OAs oxidation occurs continuously during the transport of air masses. The
470 formation yield of sulfate from SO_2 is greater than that of organic aerosol particles during
471 3~4 days of aging in the Asian pollution plume because of fast depletion of SOA
472 precursors (Dunlea et al., 2009), which is consistent to our results. In particular, this study
473 indicates that relatively less aged OAs were in equilibrium with the gas phase, through
474 which oxidation of less oxidized OAs was carried out, leading to increased OA mass
475 concentration in the CCN size range (200–400 nm). The increased O:C ratios rendered
476 particles more hygroscopic, thereby facilitating their activation as CCNs (Massoli et al.,
477 2010). Thus, climate effect of OA aging should be considered along with decreases in OA
478 mass loading when they are transported across long distances.
479

480 Table 1. Meteorological parameters and measurement summary for organic-dominated
481 and sulfate-dominated episodes.

	Organic-dominated		**Sulfate-dominated**	
	Aug. 6, 11 AM~ Aug. 7, 9 AM		Aug. 9, 1 AM~ Aug. 9, 2 PM	
Meteorological parameters				
Temp(°C)	26 ± 0.8		20 ± 0.6	
Relative humidity (%)	84 ± 7.7		96 ± 0.2	
Wind speed (m/s)	5 ± 1.6		8 ± 1.7	
Wind direction	easterly		southwesterly	
Weather mark	Cloudy		Fog	
Gaseous species				
SO_2 (ppbv)	3.1 ± 0.3		3.4 ± 0.2	
NO_2 (ppbv)	2.4 ± 0.8		0.9 ± 0.3	
CO (ppmv)	0.2 ± 0.0		0.4 ± 0.1	
O_3 (ppbv)	46 ± 22		54 ± 8	
SMPS particle mass concentration[#]				
	Ambient	**PAM**	**Ambient**	**PAM**
Total mass conc.	14.04±4.49	17.96±5.66	25.00±6.41	23.44 ± 8.91
10~50 nm	0.03±0.03	0.73±0.33	0.01±0.01	0.29±0.12
50~200 nm	5.55±2.33	5.21±2.19	7.78±2.01	9.53±2.54
200~500 nm	8.45±2.27	12.03±3.47	17.21±5.49	13.62±8.09
AMS particle mass concentrations[&]				
Sulfate	2.95 ± 1.31	4.59 ± 1.91	11.45 ± 4.65	14.66 ± 5.01
Nitrate	1.16 ± 0.85	0.52 ± 0.22	1.56 ± 1.01	0.45 ± 0.20
Ammonium	1.03 ± 0.62	1.51 ± 0.67	3.44 ± 1.36	4.07 ± 1.48
Organics	10.59± 3.71	7.97 ± 2.66	5.34 ± 1.85	3.84 ± 1.00
m/z 43	0.66 ± 0.04	0.31 ±0.01	0.24 ± 0.02	0.10 ± 0.02
m/z 44	1.47 ± 0.08	1.91 ± 0.01	0.93 ± 0.06	0.98 ± 0.05

482 # SMPS particle mass concentrations were obtained from SMPS measurements corrected
483 with a particle density of 1.4 μg cm^{-3}, and units are μg cm^{-3}.
484 [&] AMS particle mass concentrations of sulfate, nitrate, ammonium and organics were
485 obtained from MS mode AMS measurements, and units are μg cm^{-3}.

Figure Captions

Figure 1. (a) The location of the measurement site on Baengnyeong Island, the northernmost island in South Korea. The red circle indicates the measurement station location. (b) 72-hour backward trajectory for the two episodes. Green represents the organics-dominated episode during August 6, 11 AM to August 7, 9 AM, 2011, while red represents the sulfate-dominated episode during August 9, 1 AM to August 9, 2 PM, 2011.

Figure 2 (a) Aerosol particle mass concentrations from SMPS measurements for ambient and PAM aerosols. (b) Mass concentrations of major components measured by HR-ToF-AMS including organics, nitrate, sulfate, ammonium, chloride, and *m/z* 43 and *m/z* 44. Solid lines and lines with markers represent ambient aerosol particles and PAM aerosol particles, respectively. Shaded periods represent the organics-dominated episode (August 6, 11 AM to August, 7 9 AM) and the sulfate-dominated episode (August 9, 1 AM to August 9, 2 PM). The lowest mass concentration observed on August 8 was due to rain. (c) Time series of particle volume concentration measured from AMS and SMPS. Particle volume concentration from AMS was calculated with mass concentration and composition dependent density. (d) The size-separated number concentrations of ambient and PAM aerosols particles measured by SMPS.

Figure 3. SMPS mass concentration difference between PAM and ambient aerosol particles averaged for the entire sampling period.

Figure 4. Hourly measurements of SO_2, NOx, CO, O_3, EC, OC and meteorological parameters for the entire sampling period.

Figure 5. (a) AMS mass spectra of organics and SMPS mass size distribution averaged for organics-dominated episode and (b) AMS mass spectra of organics and SMPS mass size distribution averaged for sulfate-dominated episode.

512 Figure 6. AMS p-ToF size distributions of PAM and ambient particles components
513 averaged for each case.
514 Figure 7. Van Krevelen diagram for two episodes. Dashed lines represent the Van Krevelen
515 slopes, Δ(H:C)/ Δ(O:C) to show the direction of particular functional group
516 additions (Heald et al., 2010). Shaded gray areas represent the H:C and O:C ranges
517 observed in ambient OAs (Ng et al., 2011).
518 Figure 8. Comparison of O:C ratios in this study and other studies with respect to
519 photochemical age. The photochemical ages in our measurement were obtained
520 by the transport time calculated from a backward trajectory analysis and
521 photochemical aging times in the PAM reactor. Other study data were obtained
522 from Takegawa et al. (2006), Takami et al. (2007), and Dunlea et al. (2009).

Figures

Figure 1(a)

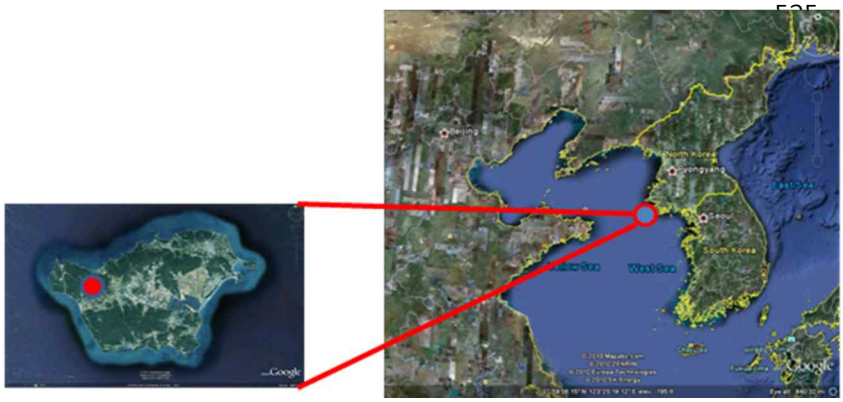

Figure 1(b)

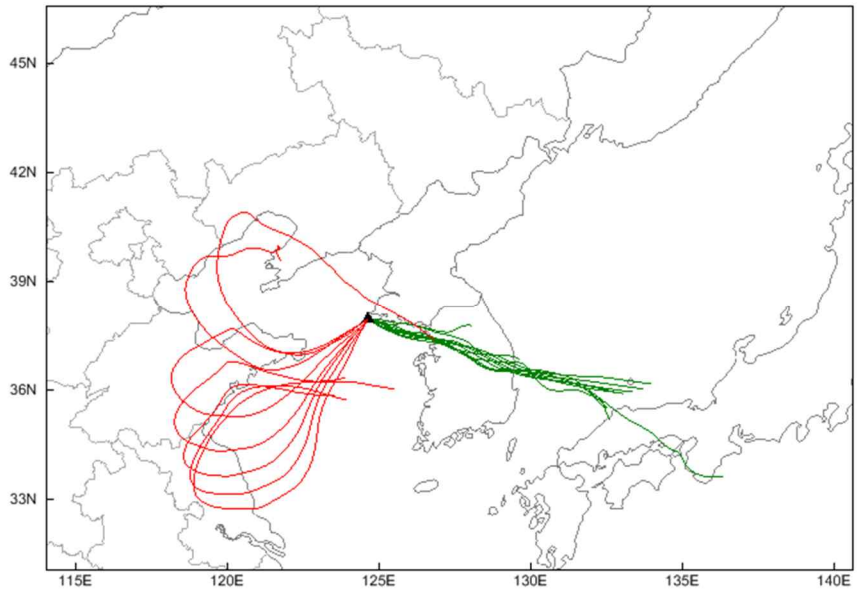

537 Figure 2(a)

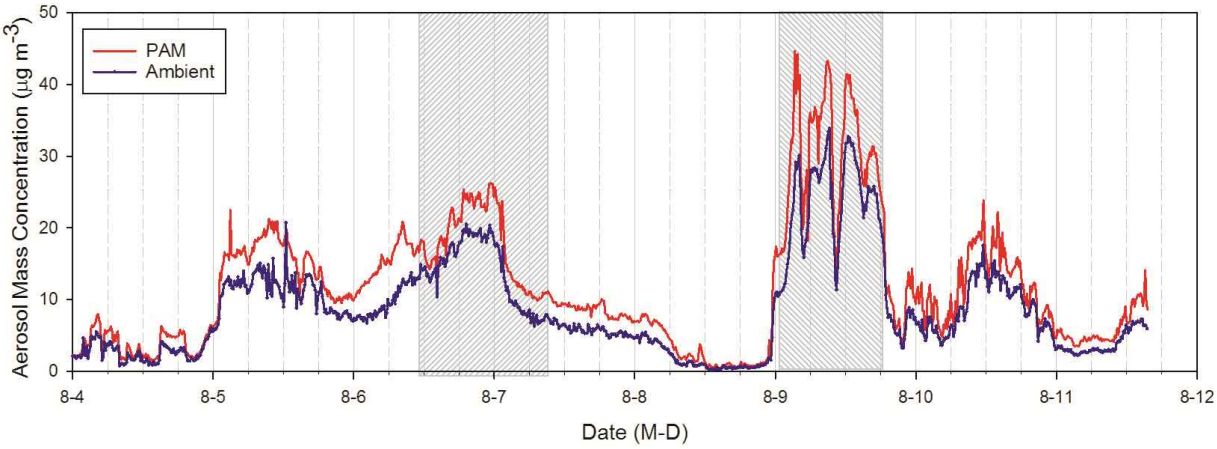

538

539

Figure 2(b)

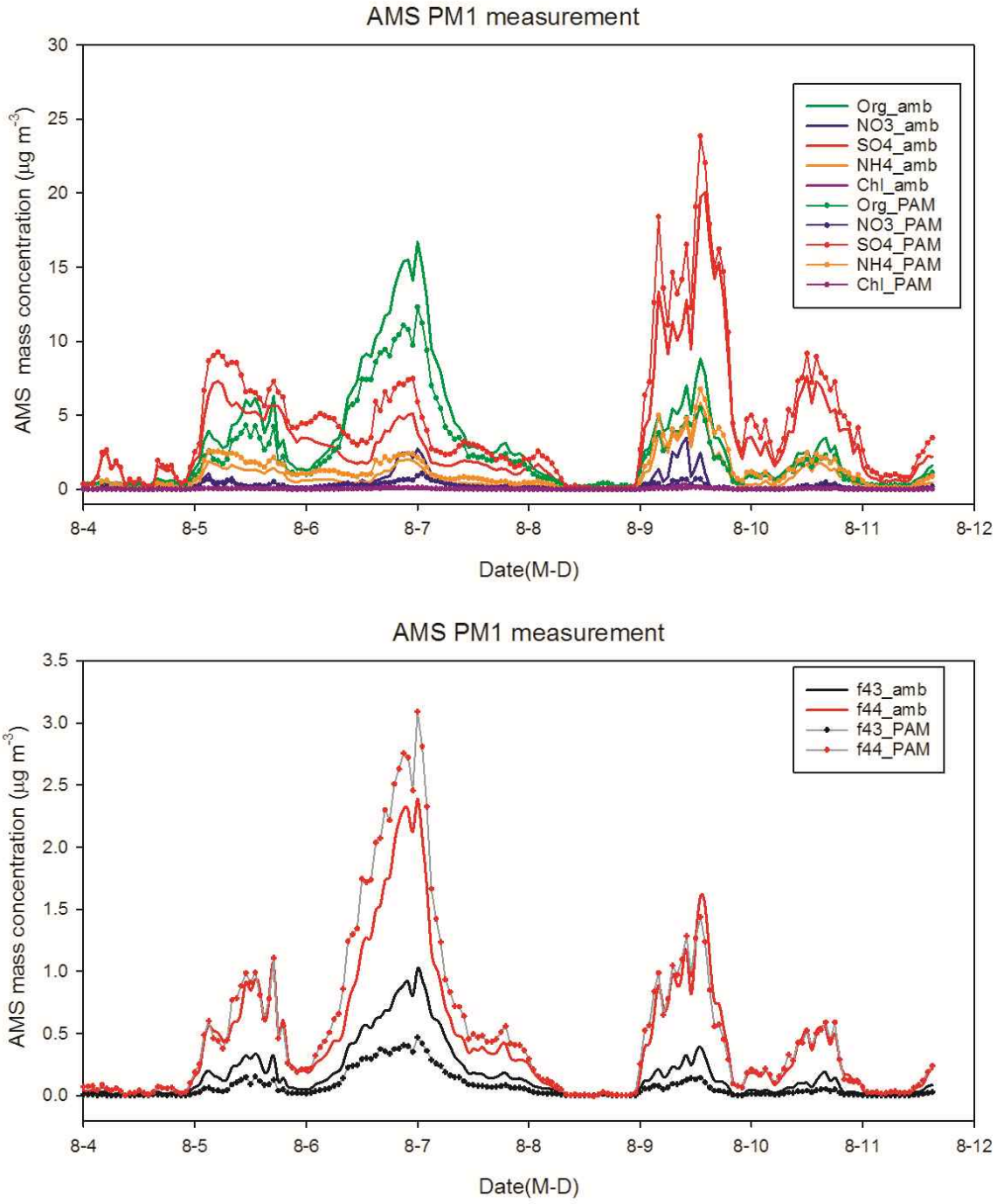
AMS PM1 measurement
AMS mass concentration (μg m-3)
Date(M-D)
Org_amb
NO3_amb
SO4_amb
NH4_amb
Chl_amb
Org_PAM
NO3_PAM
SO4_PAM
NH4_PAM
Chl_PAM
AMS PM1 measurement
AMS mass concentration (μg m-3)
Date(M-D)
f43_amb
f44_amb
f43_PAM
f44_PAM

Figure 2(c)

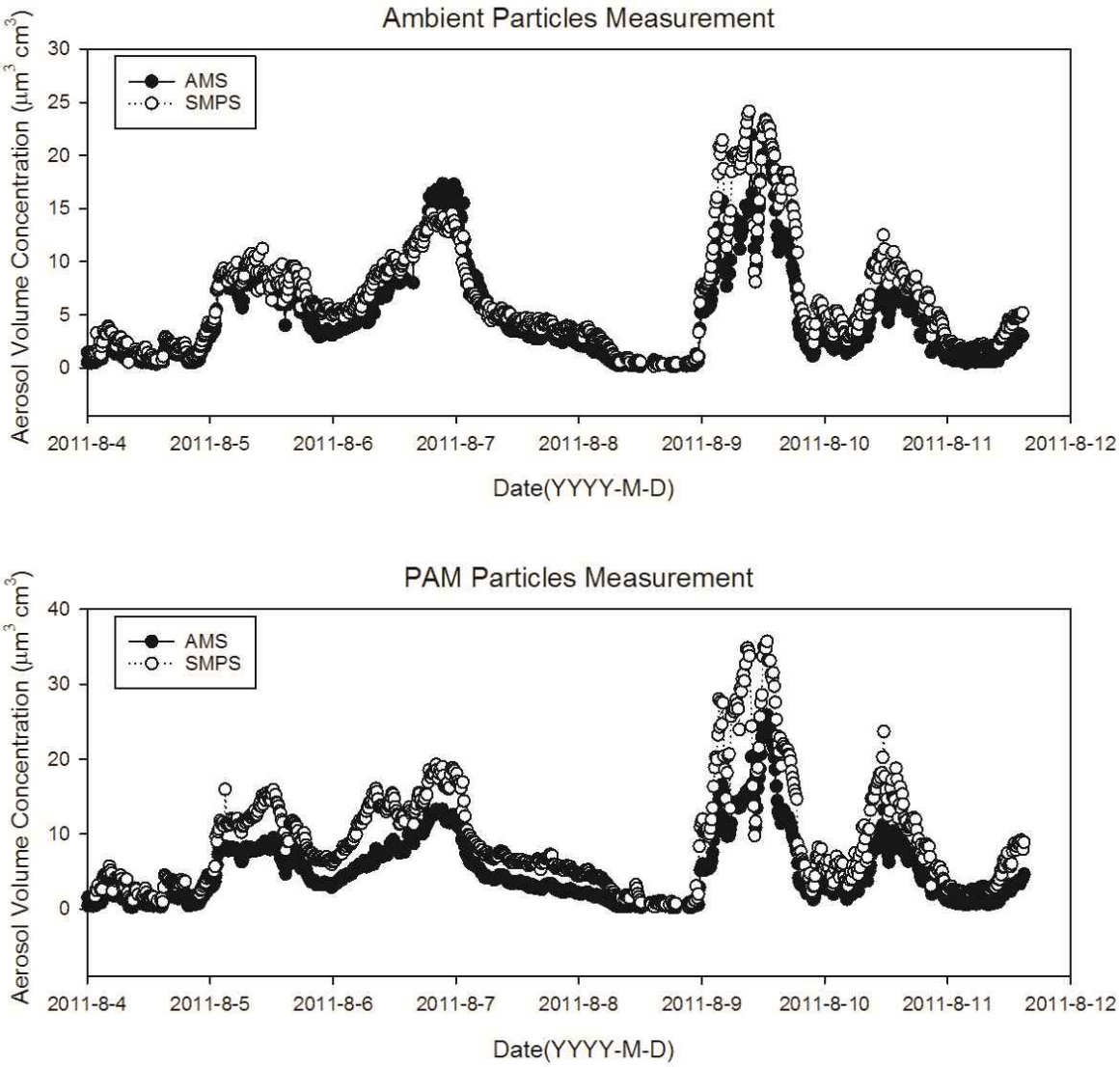
Ambient Particles Measurement
Aerosol Volume Concentration (μm3 cm3)
AMS
SMPS
0
5
10
15
20
25
30
2011-8-4
2011-8-5
2011-8-6
2011-8-7
2011-8-8
2011-8-9
2011-8-10
2011-8-11
2011-8-12
Date(YYYY-M-D)
PAM Particles Measurement
Aerosol Volume Concentration (μm3 cm3)
AMS
SMPS
0
10
20
30
40
2011-8-4
2011-8-5
2011-8-6
2011-8-7
2011-8-8
2011-8-9
2011-8-10
2011-8-11
2011-8-12
Date(YYYY-M-D)

547 Figure 2(d)

548

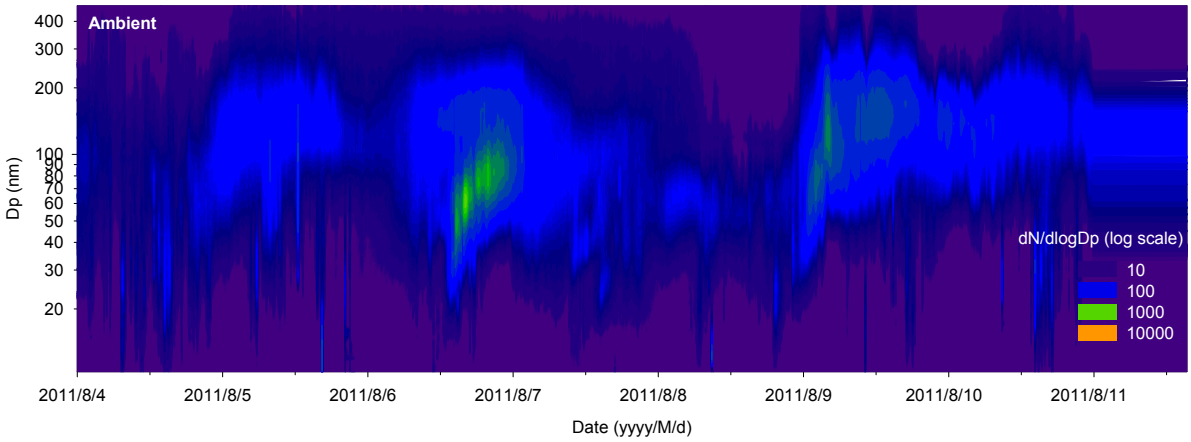

549

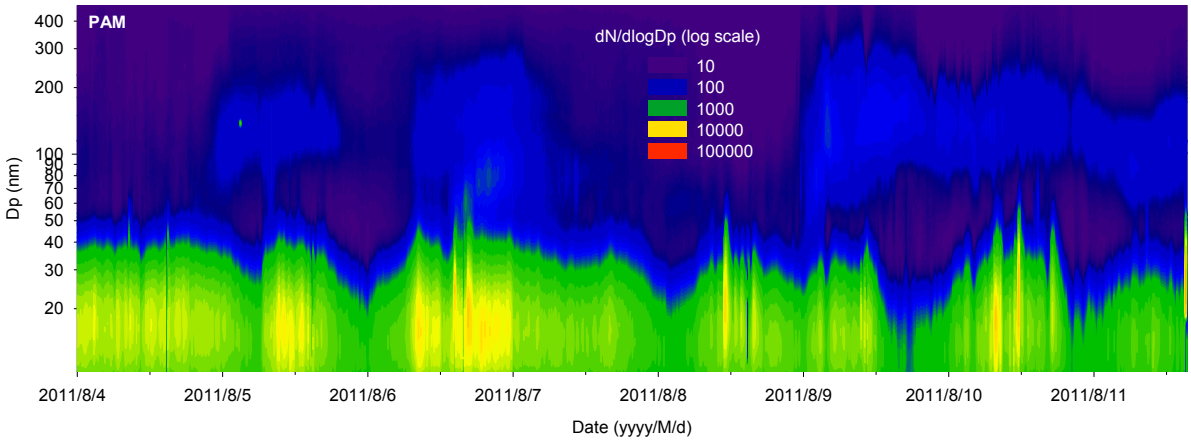

550

551

552 Figure 3.

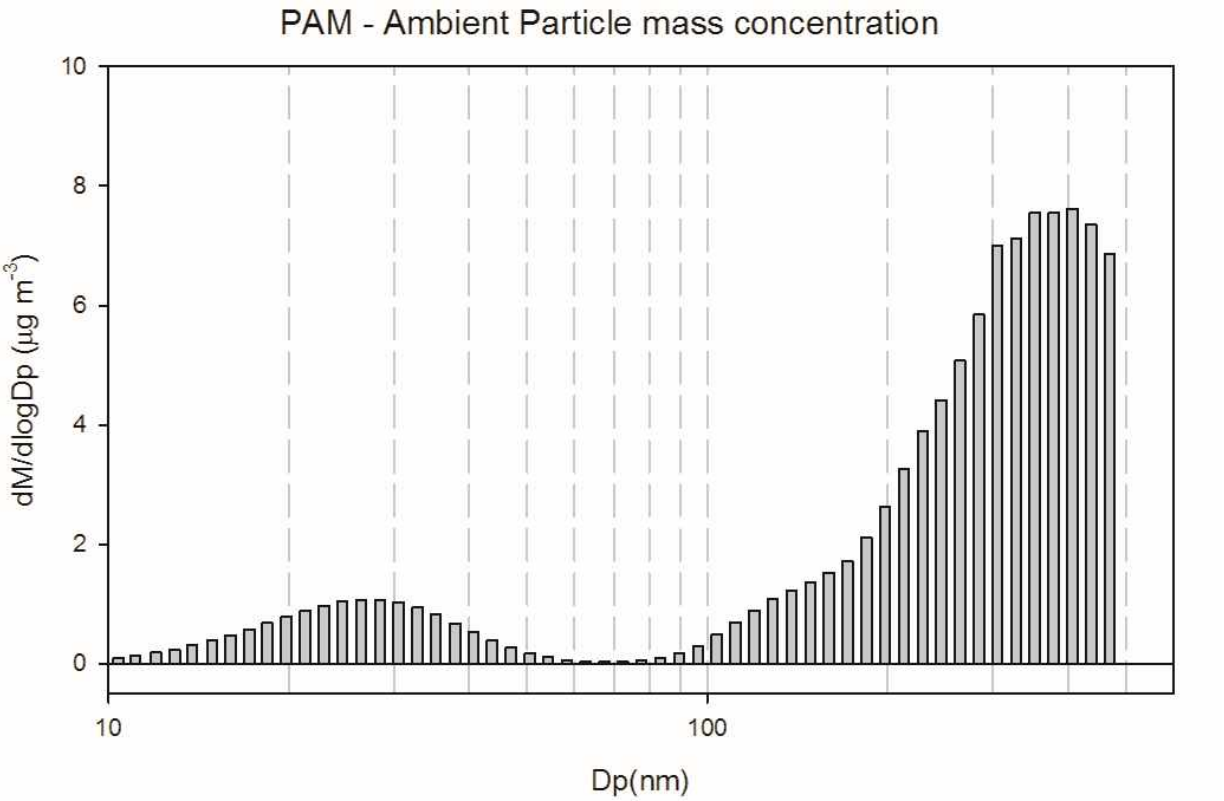

553

554 Figure 4.

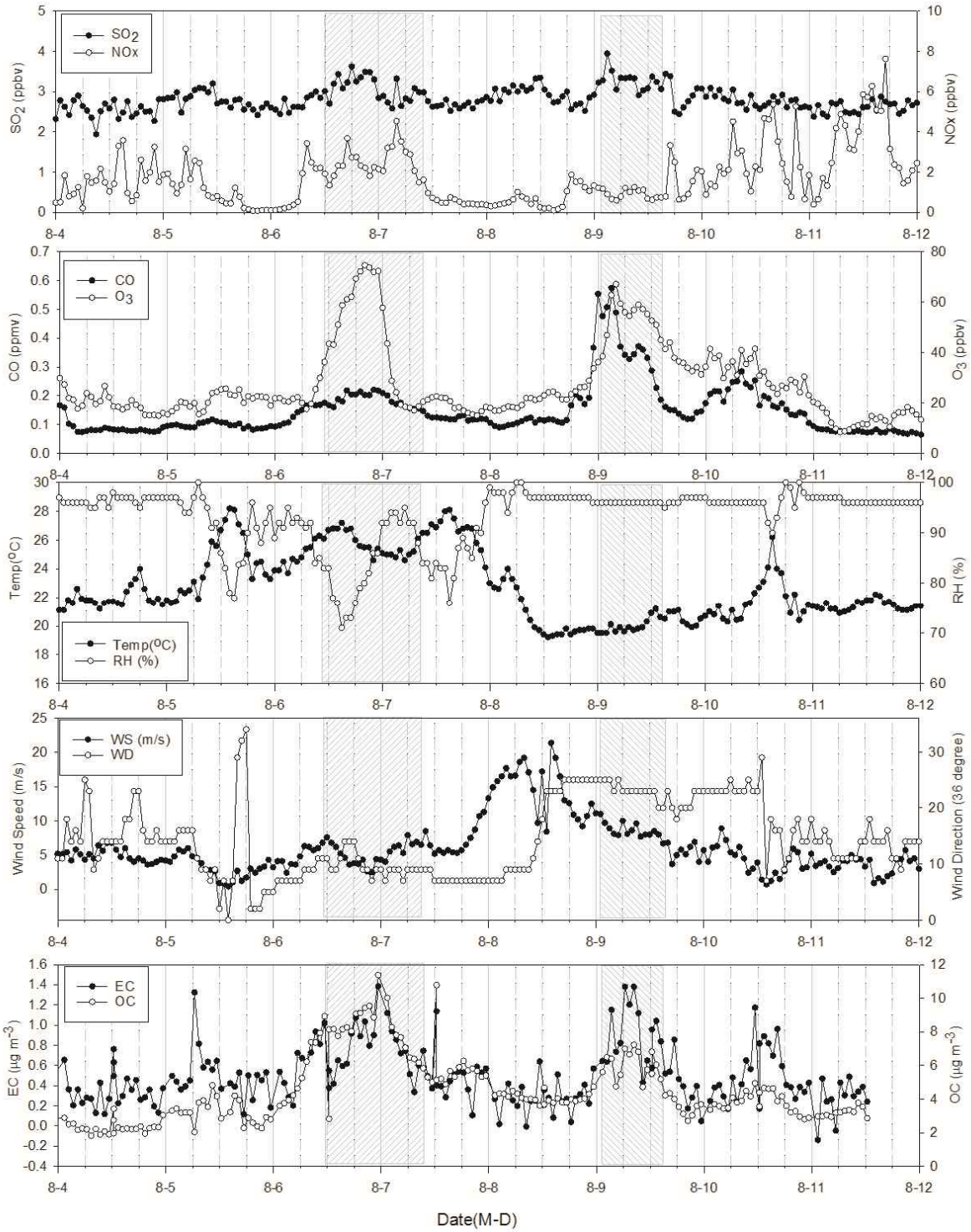

555

556

557

Figure 5(a)

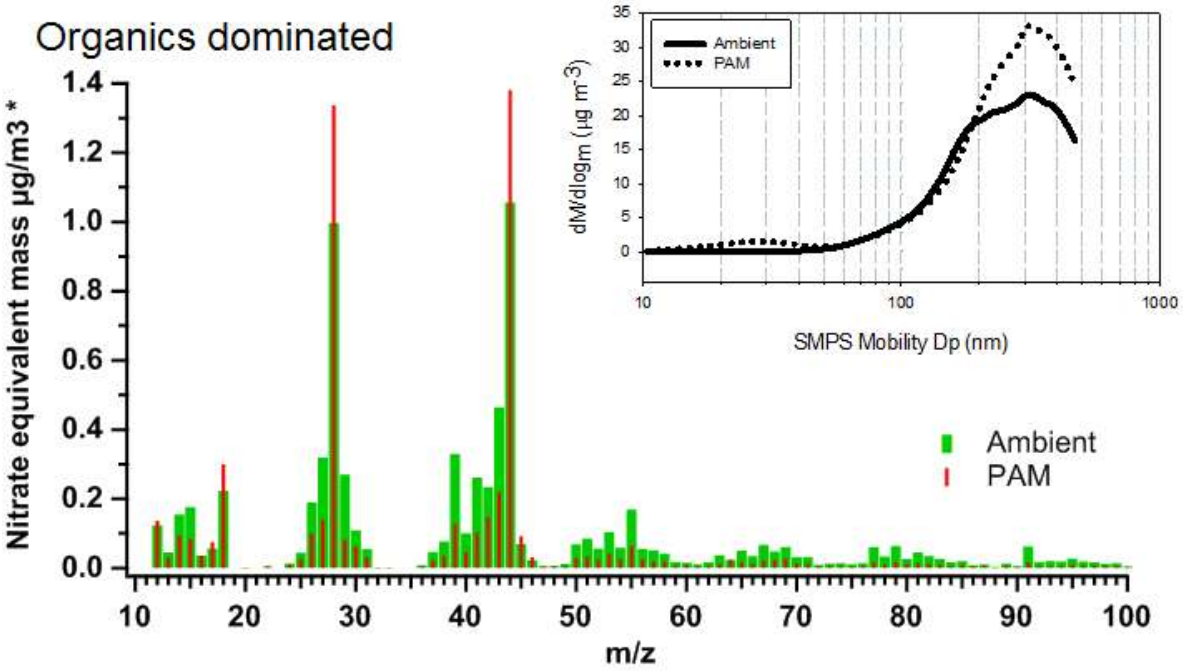

Figure 5(b)

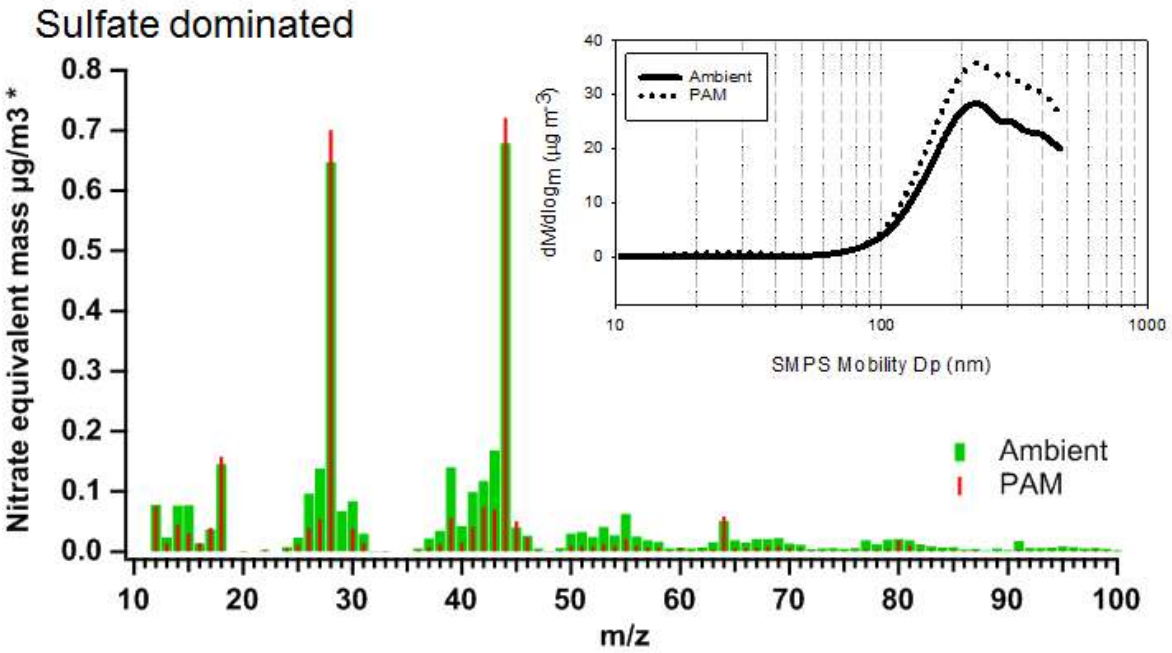

564 Figure 6.

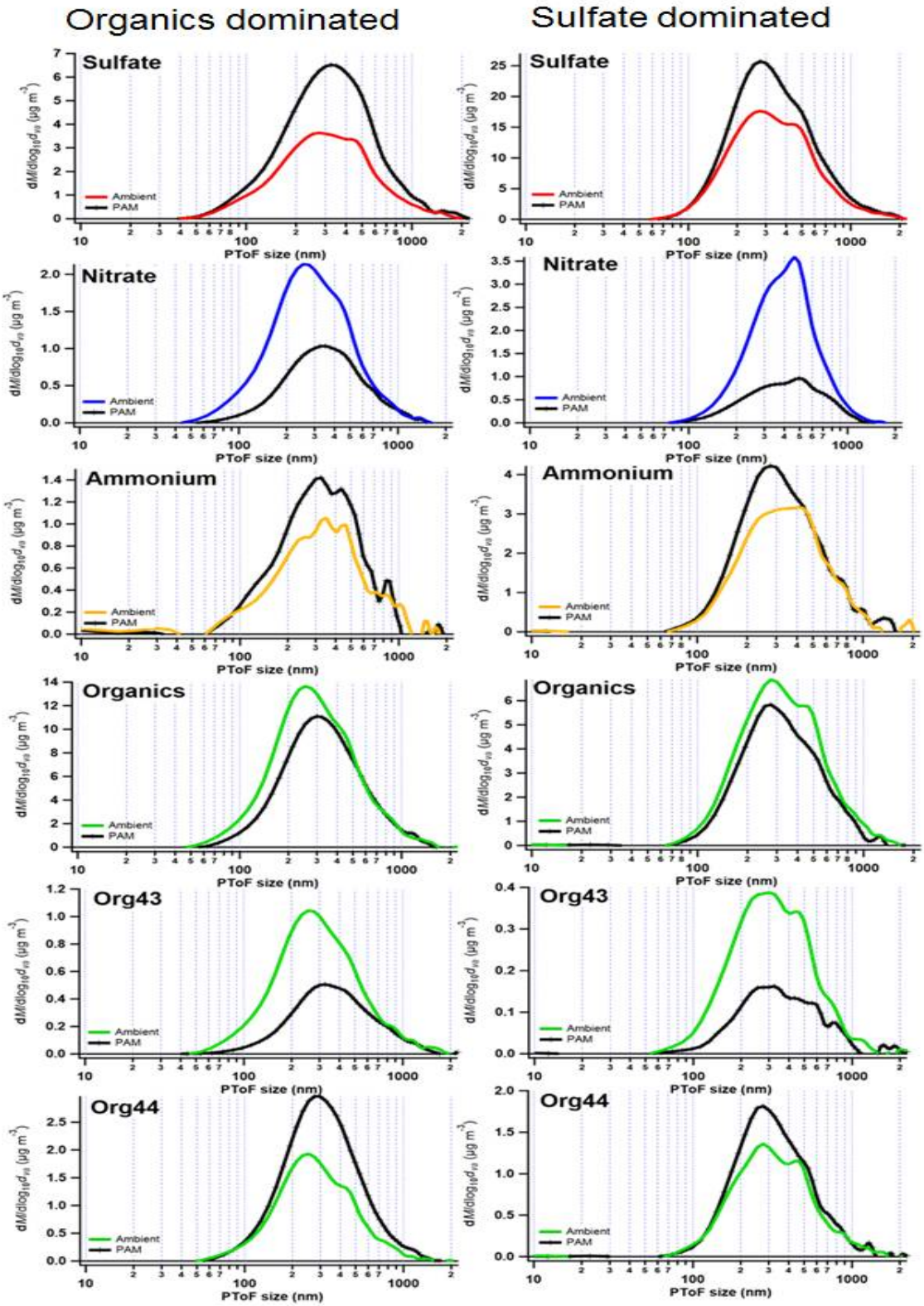

565

566 Figure 7.

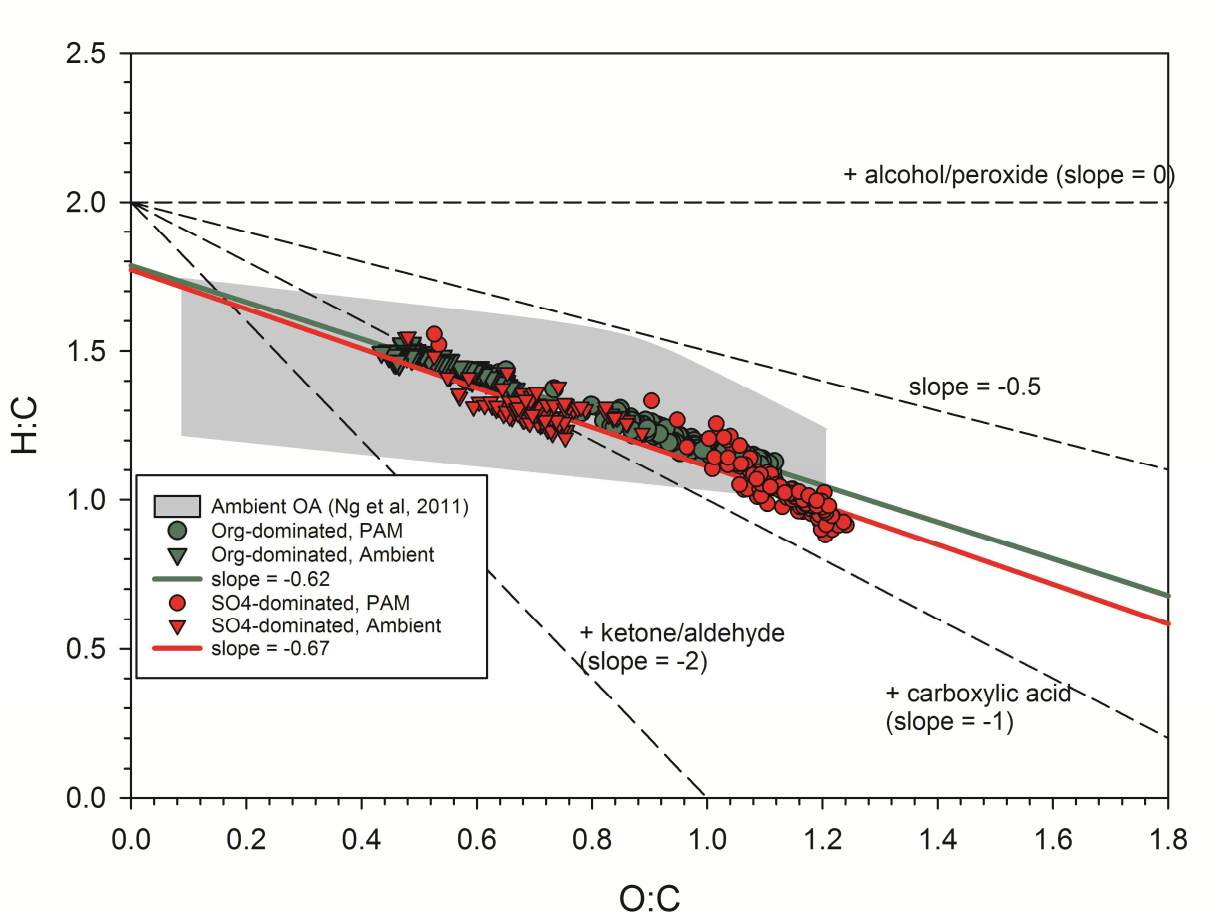

567

568

569

570 Figure 8.

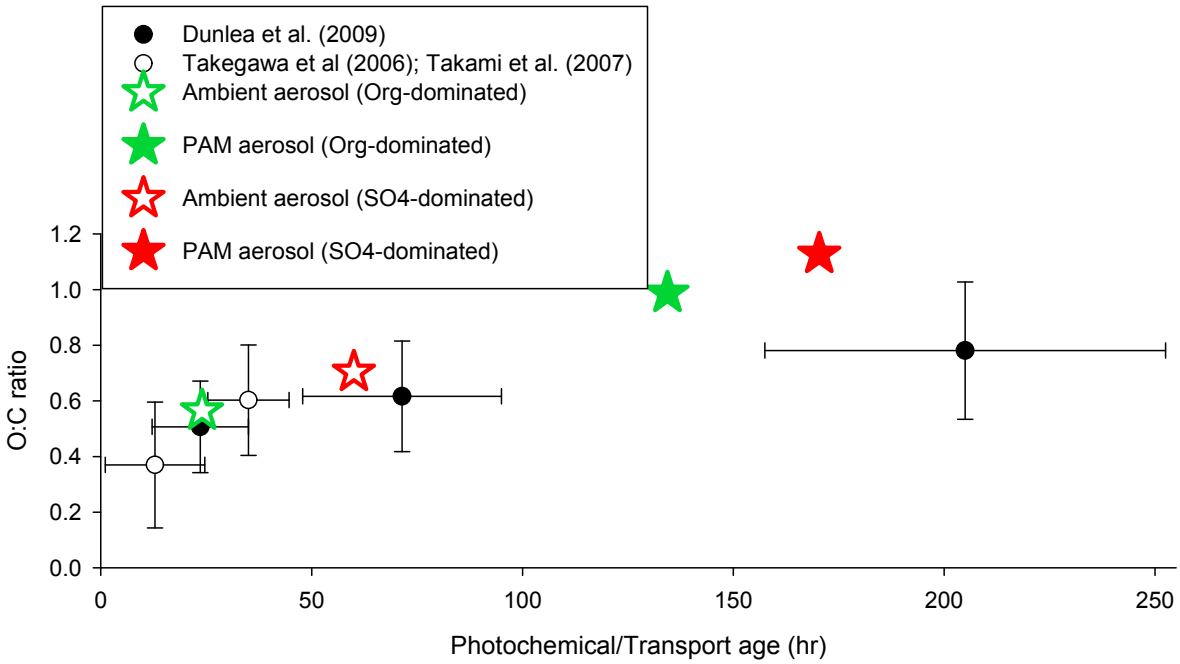

571

572

573 References

574 Aggarwal, S. G., and Kawamura, K.: Carbonaceous and inorganic composition in long-range
575 transported aerosols over northern Japan: Implication for aging of water-soluble organic
576 fraction, Atmospheric Environment, 43, 2532-2540, 2009.

577 Andreae, M. O., and Gelencser, A.: Black carbon or brown carbon? The nature of light-
578 absorbing carbonaceous aerosols, Atmos Chem Phys, 6, 3131-3148, 2006.

579 Bateman, A. P., Nizkorodov, S. A., Laskin, J., and Laskin, A.: Photolytic processing of
580 secondary organic aerosols dissolved in cloud droplets, Physical Chemistry Chemical
581 Physics, 13, 12199-12212, Doi 10.1039/C1cp20526a, 2011.

582 Brock, C. A., Hudson, P. K., Lovejoy, E. R., Sullivan, A., Nowak, J. B., Huey, L. G., Cooper, O.
583 R., Cziczo, D. J., de Gouw, J., Fehsenfeld, F. C., Holloway, J. S., Hubler, G., Lafleur, B. G.,
584 Murphy, D. M., Neuman, J. A., Nicks, D. K., Orsini, D. A., Parrish, D. D., Ryerson, T. B.,
585 Tanner, D. J., Warneke, C., Weber, R. J., and Wilson, J. C.: Particle characteristics following
586 cloud-modified transport from Asia to North America, J Geophys Res-Atmos, 109, Artn
587 D23s26 Doi 10.1029/2003jd004198, 2004.

588 Chacon-Madrid, H. J., Presto, A. A., and Donahue, N. M.: Functionalization vs.
589 fragmentation: n-aldehyde oxidation mechanisms and secondary organic aerosol
590 formation, Physical Chemistry Chemical Physics, 12, 13975-13982, Doi 10.1039/C0cp00200c,
591 2010.

592 Choi J., Kim, J., Lee, T., Choi, Y., Park, T., Oh, J., Park, J., Ahn, J., Jeon, H., Koo, Y., Kim, S.,
593 Hong, Y., and Hong, J.: A Study on Chemical Characteristics of Aerosol Composition at
594 West Inflow Regions in the Korean Peninsula I. Characteristics of PM Concentration and
595 Chemical Components, J.KOSAE., 32(5), 469-484, 2016

596 Cubison, M. J., Ortega, A. M., Hayes, P. L., Farmer, D. K., Day, D., Lechner, M. J., Brune, W.
597 H., Apel, E., Diskin, G. S., Fisher, J. A., Fuelberg, H. E., Hecobian, A., Knapp, D. J., Mikoviny,
598 T., Riemer, D., Sachse, G. W., Sessions, W., Weber, R. J., Weinheimer, A. J., Wisthaler, A., and

599 Jimenez, J. L.: Effects of aging on organic aerosol from open biomass burning smoke in
600 aircraft and laboratory studies, Atmos Chem Phys, 11, 12049-12064, DOI 10.5194/acp-11-
601 12049-2011, 2011.

602 Donahue, N. M., Robinson, A. L., Stanier, C. O., and Pandis, S. N.: Coupled partitioning,
603 dilution, and chemical aging of semivolatile organics, Environ Sci Technol, 40, 2635-2643,
604 Doi 10.1021/Es052297c, 2006.

605 Dunlea, E. J., DeCarlo, P. F., Aiken, A. C., Kimmel, J. R., Peltier, R. E., Weber, R. J., Tomlinson,
606 J., Collins, D. R., Shinozuka, Y., McNaughton, C. S., Howell, S. G., Clarke, A. D., Emmons, L.
607 K., Apel, E. C., Pfister, G. G., van Donkelaar, A., Martin, R. V., Millet, D. B., Heald, C. L., and
608 Jimenez, J. L.: Evolution of Asian aerosols during transpacific transport in INTEX-B, Atmos
609 Chem Phys, 9, 7257-7287, 2009.

610 Feiner, P., Brune, W., Miller, D., Zhang, L., Cohen, R., Romer, P., Goldstein, A., Keutsch, F.,
611 Skog, K., Wennberg, P., Nguyen, T., Teng, A., DeGouw, J., Koss, A., Wild, R., Brown, S.,
612 Guenther, A., Edgerton, E., Baumann, K., Fry, J.: Testing Atmospheric Oxidation in an
613 Alabama Forest. J. Atmos. Sci. 73(12), 4699-4710, 2016.

614 George, I. J., and Abbatt, J. P. D.: Chemical evolution of secondary organic aerosol from
615 OH-initiated heterogeneous oxidation, Atmos Chem Phys, 10, 5551-5563, DOI
616 10.5194/acp-10-5551-2010, 2010.

617 Gilardoni, S., Massoli, P., Giulianelli, L., Rinaldi, M., Paglione, M., Pollini, F., Lanconelli, C.,
618 Poluzzi, V., Carbone, S., Hilamo, R., Russell, L.M., Facchini, M.C., Fuzzi, S.: Fog scavenging of
619 organic and inorganic aerosol in the Po Valley, Atmos. Chem. Phys., 14, 6967-6981, 2014.

620 Hallquist, M., Wenger, J. C., Baltensperger, U., Rudich, Y., Simpson, D., Claeys, M., Dommen,
621 J., Donahue, N. M., George, C., Goldstein, A. H., Hamilton, J. F., Herrmann, H., Hoffmann, T.,
622 Iinuma, Y., Jang, M., Jenkin, M. E., Jimenez, J. L., Kiendler-Scharr, A., Maenhaut, W.,
623 McFiggans, G., Mentel, T. F., Monod, A., Prevot, A. S. H., Seinfeld, J. H., Surratt, J. D.,
624 Szmigielski, R., and Wildt, J.: The formation, properties and impact of secondary organic

625 aerosol: current and emerging issues, Atmos Chem Phys, 9, 5155-5236, 2009.

626 Hayes, P.L., Carlton, A.G., Baker, K.R., Ahmadov, R., Washenfelder, R.A., Alvarez, S.,
627 Rappenglück, Gilman, J.B., Kuster, W.C., de Gouw, J.A., Zotter, P., Prévôt, A.S.H., Szidat, S.,
628 Kleindienst, T.E., Offenber, J.H., Ma, P.K., Jimenez, J.L.: Modeling the formation and aging of
629 secondary organic aerosols in Los Angeles during CalNex 2010, Atmos. Chem. Phys., 15,
630 5773-5801, 2015.

631 Heald, C. L., Kroll, J. H., Jimenez, J. L., Docherty, K. S., DeCarlo, P. F., Aiken, A. C., Chen, Q.,
632 Martin, S. T., Farmer, D. K., and Artaxo, P.: A simplified description of the evolution of
633 organic aerosol composition in the atmosphere, Geophys Res Lett, 37, Artn L08803, Doi
634 10.1029/2010gl042737, 2010.

635 Henry, K. M., and Donahue, N. M.: Photochemical Aging of alpha-Pinene Secondary
636 Organic Aerosol: Effects of OH Radical Sources and Photolysis, J. Phys. Chem. A, 116, 5932-
637 5940, Doi 10.1021/Jp210288s, 2012.

638 Hu, W.W., Hu, M., Yuan, B., Jimenez, J.L., Tang, Q., Peng, J.F., Hu, W., Shao, M., Wang, M.,
639 Zeng, L.M., Wu, Y.S., Gong, Z.H., Huang, X.F., and He, L.Y.: Insights on organic aerosol aging
640 and the influence of coal combustion at a regional receptor site of central eastern China,
641 Atmos. Chem. Phys., 13, 10095-10112, 2013.

642 Hu, W., Palm, B.B., Day, D.A., Campuzano-Jost, P., Krechmer, J.E., Peng, Z., de Sá, S.S.,
643 Martin, S.T., Alexander, M.L., Baumann, K., Hacker, L., Kiendler-Scharr, A., Koss, A.R., de
644 Gouw, J.A., Goldstein, A.H., Seco, R., Sjostedt, S.J., Park, J.-H., Guenther, A.B., Kim, S.,
645 Canonaco, R., Prévôt, A.S.H., Brune, W.H., Jimenez, J.L.: Volatility and lifetime against OH
646 heterogeneous reaction of ambient isoprene-epoxydiols-derived secondary organic aerosol
647 (IEPOX-SOA), Atmos. Chem. Phys., 16, 11563-11580, 2016.

648 Huang, R.J., Zhang, Y., Bozzetti, C., Ho, K.F., Cao, J.J., Han, Y., Daellenbach, K.R., Slowik, J.G.,
649 Platt, S.M., Canonaco, F., Zotter, P., Wolf, R., Pieber, S.M., Bruns, E.A., Crippa, M., Ciarelli, G.,
650 Piazzalunga, A., Schwikowski, M., Abbaszade, G., Schnelle-Kreis, J., Zimmermann, R., An, Z.,

651 Szidat, S., Baltensperger, U., Haddad, I.E., and Prevot, A.S.H.: High secondary aerosol
652 contribution to particulate pollution during haze events in China, Nature, 514, 218-222,
653 2014.

654 Jang, M., Czoschke, N. M., Northcross, A. L., Cao, G., and Shaof, D.: SOA formation from
655 partitioning and heterogeneous reactions: Model study in the presence of inorganic
656 species, Environ Sci Technol, 40, 3013-3022, Doi 10.1021/Es0511220, 2006.

657 Jang, M. S., Czoschke, N. M., Lee, S., and Kamens, R. M.: Heterogeneous atmospheric
658 aerosol production by acid-catalyzed particle-phase reactions, Science, 298, 814-817, DOI
659 10.1126/science.1075798, 2002.

660 Jimenez, J. L., Canagaratna, M. R., Donahue, N. M., Prevot, A. S. H., Zhang, Q., Kroll, J. H.,
661 DeCarlo, P. F., Allan, J. D., Coe, H., Ng, N. L., Aiken, A. C., Docherty, K. S., Ulbrich, I. M.,
662 Grieshop, A. P., Robinson, A. L., Duplissy, J., Smith, J. D., Wilson, K. R., Lanz, V. A., Hueglin,
663 C., Sun, Y. L., Tian, J., Laaksonen, A., Raatikainen, T., Rautiainen, J., Vaattovaara, P., Ehn, M.,
664 Kulmala, M., Tomlinson, J. M., Collins, D. R., Cubison, M. J., Dunlea, E. J., Huffman, J. A.,
665 Onasch, T. B., Alfarra, M. R., Williams, P. I., Bower, K., Kondo, Y., Schneider, J., Drewnick, F.,
666 Borrmann, S., Weimer, S., Demerjian, K., Salcedo, D., Cottrell, L., Griffin, R., Takami, A.,
667 Miyoshi, T., Hatakeyama, S., Shimono, A., Sun, J. Y., Zhang, Y. M., Dzepina, K., Kimmel, J. R.,
668 Sueper, D., Jayne, J. T., Herndon, S. C., Trimborn, A. M., Williams, L. R., Wood, E. C.,
669 Middlebrook, A. M., Kolb, C. E., Baltensperger, U., and Worsnop, D. R.: Evolution of Organic
670 Aerosols in the Atmosphere, Science, 326, 1525-1529, DOI 10.1126/science.1180353, 2009.

671 Kang, E., Root, M. J., Toohey, D. W., and Brune, W. H.: Introducing the concept of Potential
672 Aerosol Mass (PAM), Atmos Chem Phys, 7, 5727-5744, 2007.

673 Kang, E., Brune, W. H., Kim, S., Yoon, S. C., Jung, M., and Lee, M.: A preliminary PAM
674 measurement of ambient air at Gosan, Jeju to study the secondary aerosol forming
675 potential, Journal of Korean Society for Atmospheric Environment, 27, 11, 2011a.

676 Kang, E., Toohey, D. W., and Brune, W. H.: Dependence of SOA oxidation on organic

677 aerosol mass concentration and OH exposure: experimental PAM chamber studies, Atmos
678 Chem Phys, 11, 1837-1852, DOI 10.5194/acp-11-1837-2011, 2011b.

679 Kang, E., Han, J., Lee, M., Lee, G., Kim, J.C.: Chemical characteristics of size-resolved
680 aerosols from Asian dust and haze episode in Seoul metropolitan city, Atmos. Res., 127,
681 34-46, 2013.

682 Kessler, S. H., Nah, T., Daumit, K. E., Smith, J. D., Leone, S. R., Kolb, C. E., Worsnop, D. R.,
683 Wilson, K. R., and Kroll, J. H.: OH-Initiated Heterogeneous Aging of Highly Oxidized
684 Organic Aerosol, J Phys Chem A, 116, 6358-6365, Doi 10.1021/Jp212131 m, 2012.

685 Kim, Y. J., Woo, J.-H., Ma, Y.-I., Kim, S., Nam, J. S., Sung, H., Choi, K.-C., Seo, J., Kim, J. S.,
686 Kang, C.-H., Lee, G., Ro, C.-U., Chang, D., and Sunwoo, Y.: Chemical characteristics of long-
687 range transport aerosol at background sites in Korea, Atmospheric Environment, 43, 5556-
688 5566, 2009.

689 King, S. M., Rosenoern, T., Shilling, J. E., Chen, Q., Wang, Z., Biskos, G., McKinney, K. A.,
690 Pöschl, U., and Martin, S. T.: Cloud droplet activation of mixed organic-sulfate particles
691 produced by the photooxidation of isoprene, Atmos. Chem. Phys., 10, 3953-3964,
692 10.5194/acp-10-3953-2010, 2010.

693 Kroll, J. H., and Seinfeld, J. H.: Chemistry of secondary organic aerosol: Formation and
694 evolution of low-volatility organics in the atmosphere, Atmospheric Environment, 42, 3593-
695 3624, DOI 10.1016/j.atmosenv.2008.01.003, 2008.

696 Kroll, J. H., Smith, J. D., Che, D. L., Kessler, S. H., Worsnop, D. R., and Wilson, K. R.:
697 Measurement of fragmentation and functionalization pathways in the heterogeneous
698 oxidation of oxidized organic aerosol, Physical Chemistry Chemical Physics, 11, 8005-8014,
699 Doi 10.1039/B905289e, 2009.

700 La, Y.S., Camredon, M., Ziemann, P.J., Valorso, R., Matsunaga, A., Lannuque, V., Lee-Taylor,
701 J., Hodzic, A., Madronich, S., and Aumont, B.: Impact of chamber wall loss of gaseous
702 organic compounds on secondary organic aerosol formation: explicit modeling of SOA

703 formation from alkane and alkene oxidation, Atmos. Chem. Phys., 16, 1417-1431,
704 2016.Lambe, A. T., Ahern, A. T., Williams, L. R., Slowik, J. G., Wong, J. P. S., Abbatt, J. P. D.,
705 Brune, W. H., Ng, N. L., Wright, J. P., Croasdale, D. R., Worsnop, D. R., Davidovits, P., and
706 Onasch, T. B.: Characterization of aerosol photooxidation flow reactors: heterogeneous
707 oxidation, secondary organic aerosol formation and cloud condensation nuclei activity
708 measurements, Atmos Meas Tech, 4, 445-461, DOI 10.5194/amt-4-445-2011, 2011.

709 Lambe, A. T., Onasch, T. B., Croasdale, D. R., Wright, J. P., Martin, A. T., Franklin, J. P.,
710 Massoli, P., Kroll, J. H., Canagaratna, M. R., Brune, W. H., Worsnop, D. R., and Davidovits, P.:
711 Transitions from Functionalization to Fragmentation Reactions of Laboratory Secondary
712 Organic Aerosol (SOA) Generated from the OH Oxidation of Alkane Precursors, Environ Sci
713 Technol, 46, 5430-5437, Doi 10.1021/Es300274t, 2012.

714 Lambe, A. T., Chhabra, P.S., Onasch,T.B., Brune, W.H., Hunter, J.F., Kroll, J.H., Cummings,
715 M.J., Brogan, J.F., Parmar, Y., Worsnop, D.R., Kolb, C.E., and Davidovits, P.: Effect of oxidant
716 concentration, exposure time and seed particles on secondary organic aerosol chemical
717 composition and yield. Atmos. Chem. Phys.,15, 3063-3075, 2015.

718 Lee, M., Song, M., Moon, K. J., Han, J. S., Lee, G., and Kim, K. R.: Origins and chemical
719 characteristics of fine aerosols during the northeastern Asia regional experiment
720 (atmospheric brown cloud east Asia regional experiment 2005), J Geophys Res-Atmos, 112,
721 Artn D22s29 Doi 10.1029/2006jd008210, 2007.

722 Lee, T., Choi, J., Lee, G., Ahn, J., Park, J., Atwood, S.A., Schurman, M., Choi, Y., Chung, Y.,
723 Collett, Jr. J.L.: Characterization of Aerosol Composition, Concentrations, and Sources at
724 Baengnyeong Island, Korea using an Aerosol Mass Spectrometer, Atmospheric
725 Environment 120, 297-306, 2015.

726 Li, Z., Li, C., Chen, H., Tsay, S.C., Holben, B., Huang, J., Li, B., Maring, H., Qian, Y., Shi, G., Xia,
727 X., Yin, Y., Zheng, Y., Zhuang, G.: East Asian studies of tropospheric aerosols and their
728 impact on regional climate (EAST-AIRC): An overview, J. Geophys. Re., 116, D00L34,
729 doi:10.1029/2010JD015257, 2011.

730 Lim, S., Lee, M., Kim, S.W., Yoon, S.C., Lee, G., and Lee, Y.J.: Absorption and scattering
731 properties of organic carbon versus sulfate dominant aerosols at Gosan climate
732 observatory in Northeast Asia, Atmos. Chem. Phys., 14, 7781-7793, 2014.

733 Link, M.F., Kim, J., Park, G., Lee, T., Park, T., Babar, Z.B., Sung, K., Kim, P., Kang, W., Kim, J.,
734 Choi, Y., Son, J., Lim, H.-J., Farmer, D.K.: Elevated production of NH_4NO_3 from the
735 photochemical processing of vehicle exhaust: Implications for air quality in the Seoul
736 Metropolitan Region, Atmos. Environ., 156, 95-101, 2017.

737 MaMurry, P.H. and Grosjean, D.: Gas and aerosol wall losses in Teflon film smog chambers,
738 Environ. Sci. Technol., 19(12), 1176-1182, 1985.

739 Mao, J., Ren, X., Chen, S., Brune, W.H., Chen, Z., Martinez, M., Harder, H., Lefer, B.,
740 Rappenglueck, B., Flynn, J., Leuchner, M.,: Atmospheric oxidation capacity in the summer of
741 Houston 2006: Comparison with summer measurements in other metropolitan studies,
742 Atmospheric Environment, 44, 4107–4115, 2010.

743 Massoli, P., Lambe, A. T., Ahern, A. T., Williams, L. R., Ehn, M., Mikkila, J., Canagaratna, M. R.,
744 Brune, W. H., Onasch, T. B., Jayne, J. T., Petaja, T., Kulmala, M., Laaksonen, A., Kolb, C. E.,
745 Davidovits, P., and Worsnop, D. R.: Relationship between aerosol oxidation level and
746 hygroscopic properties of laboratory generated secondary organic aerosol (SOA) particles,
747 Geophys. Res. Lett, 37, Artn L24801, Doi 10.1029/2010gl045258, 2010.

748 McGraw, R., Saunders, J.H.: A condensation feedback mechanism for oscillatory nucleation
749 and growth, Aerosol Science and Technology, 3(4), 367-380, 1984.

750 Middlebrook, A.M., R. Bahreini, J.L. Jimenez, and M.R. Canagaratna. Evaluation of
751 Composition-Dependent Collection Efficiencies for the Aerodyne Aerosol Mass
752 Spectrometer using Field Data. Aerosol Sci. Technol., 46, 258–271, 2012.Mohr, C., DeCarlo,
753 P. F., Heringa, M. F., Chirico, R., Slowik, J. G., Richter, R., Reche, C., Alastuey, A., Querol, X.,
754 Seco, R., Penuelas, J., Jimenez, J. L., Crippa, M., Zimmermann, R., Baltensperger, U., and
755 Prevot, A. S. H.: Identification and quantification of organic aerosol from cooking and other

sources in Barcelona using aerosol mass spectrometer data, Atmos Chem Phys, 12, 1649-1665, DOI 10.5194/acp-12-1649-2012, 2012.

Morgan, W. T., Allan, J. D., Bower, K. N., Esselborn, M., Harris, B., Henzing, J. S., Highwood, E. J., Kiendler-Scharr, A., McMeeking, G. R., Mensah, A. A., Northway, M. J., Osborne, S., Williams, P. I., Krejci, R., and Coe, H.: Enhancement of the aerosol direct radiative effect by semi-volatile aerosol components: airborne measurements in North-Western Europe, Atmos Chem Phys, 10, 8151-8171, DOI 10.5194/acp-10-8151-2010, 2010.

Ng, N. L., Canagaratna, M. R., Zhang, Q., Jimenez, J. L., Tian, J., Ulbrich, I. M., Kroll, J. H., Docherty, K. S., Chhabra, P. S., Bahreini, R., Murphy, S. M., Seinfeld, J. H., Hildebrandt, L., Donahue, N. M., DeCarlo, P. F., Lanz, V. A., Prevot, A. S. H., Dinar, E., Rudich, Y., and Worsnop, D. R.: Organic aerosol components observed in Northern Hemispheric datasets from Aerosol Mass Spectrometry, Atmos Chem Phys, 10, 4625-4641, DOI 10.5194/acp-10-4625-2010, 2010.

Ng, N. L., Canagaratna, M. R., Jimenez, J. L., Chhabra, P. S., Seinfeld, J. H., and Worsnop, D. R.: Changes in organic aerosol composition with aging inferred from aerosol mass spectra, Atmos Chem Phys, 11, 6465-6474, DOI 10.5194/acp-11-6465-2011, 2011.

Ortega, A.M., Day, D.A., Cubison, M.J., Brune, W.H., Bon, D., de Gouw, J.A., Jimenez, J,L.: Secondary organic aerosol formation and primary organic aerosol oxidation from biomass-burning smoke in a flow reactor during FLAME-3, Atmos. Chem. Phys., 13, 11551-11571, 2013.

Ortega, A. M., Hayes, P. L., Peng, Z., Palm, B. B., Hu, W., Day, D. A., Li, R., Cubison, M. J., Brune, W. H., Graus, M., Warneke, C., Gilman, J. B., Kuster, W. C., de Gouw, J., Gutiérrez-Montes, C., and Jimenez, J. L.: Real-time measurements of secondary organic aerosol formation and aging from ambient air in an oxidation flow reactor in the Los Angeles area, Atmos. Chem. Phys., 16, 7411-7433, doi:10.5194/acp-16-7411-2016, 2016.

Palm, B. B., Campuzano-Jost, P., Ortega, A. M., Day, D. A., Kaser, L., Jud, W., Karl, T., Hansel,

782 A., Hunter, J. F., Cross, E. S., Kroll, J. H., Peng, Z., Brune, W. H., and Jimenez, J. L.: In situ
783 secondary organic aerosol formation from ambient pine forest air using an oxidation flow
784 reactor, Atmos. Chem. Phys., 16, 2943-2970, doi:10.5194/acp-16-2943-2016, 2016.

785 Palm, B. B., Campuzano-Jost, P., Day, D. A., Ortega, A. M., Fry, J. L., Brown, S. S., Zarzana, K.
786 J., Dube, W., Wagner, N. L., Draper, D. C., Kaser, L., Jud, W., Karl, T., Hansel, A., Gutiérrez-
787 Montes, C., and Jimenez, J. L.: Secondary organic aerosol formation from in situ OH, O3,
788 and NO3 oxidation of ambient forest air in an oxidation flow reactor, Atmos. Chem. Phys.
789 Discuss., doi:10.5194/acp-2016-1080, 2017.

790 Peng, Z., Day, D. A., Stark, H., Li, R., Lee-Taylor, J., Palm, B. B., Brune, W. H., and Jimenez, J.
791 L.: HOx radical chemistry in oxidation flow reactors with low-pressure mercury lamps
792 systematically examined by modeling, Atmos. Meas. Tech., 8, 4863-4890, doi:10.5194/amt-
793 8-4863-2015, 2015.

794 Peng, Z., Day, D. A., Ortega, A. M., Palm, B. B., Hu, W., Stark, H., Li, R., Tsigaridis, K., Brune,
795 W. H., and Jimenez, J. L.: Non-OH chemistry in oxidation flow reactors for the study of
796 atmospheric chemistry systematically examined by modeling, Atmos. Chem. Phys., 16,
797 4283-4305, doi:10.5194/acp-16-4283-2016, 2016.

798 Peltier, R. E., Hecobian, A. H., Weber, R. J., Stohl, A., Atlas, E. L., Riemer, D. D., Blake, D. R.,
799 Apel, E., Campos, T., and Karl, T.: Investigating the sources and atmospheric processing of
800 fine particles from Asia and the Northwestern United States measured during INTEX B,
801 Atmos. Chem. Phys., 8, 1835-1853, 2008.

802 Ramana, M. V., Ramanathan, V., Feng, Y., Yoon, S. C., Kim, S. W., Carmichael, G. R., and
803 Schauer, J. J.: Warming influenced by the ratio of black carbon to sulfate and the black-
804 carbon source, Nat Geosci, 3, 542-545, Doi 10.1038/Ngeo918, 2010.

805 Richter, A., Burrows, J. P., Nuss, H., Granier, C., and Niemeier, U.: Increase in tropospheric
806 nitrogen dioxide over China observed from space, Nature, 437, 129-132,
807 10.1038/nature04092, 2005.

808 Salimi, F., Crilley, L. R., Stevanovic, S., Ristovski, Z., Mazaheri, M., He, C., Johnson, G., Ayoko,
809 G., and Morawska, L.: Insights into the growth of newly formed particles in a subtropical
810 urban environment, Atmos. Chem. Phys., 15, 13475-13485, https://doi.org/10.5194/acp-15-
811 13475-2015, 2015.

812 Song, M., Lee, M., Kim, J.H., Yum, S.S., Lee, G., Kim, K-R.: New particle formation and
813 growth in relation to vertical mixing and chemical species during ABC-EAREX2005, Atmos.
814 Res., 97, 359-370, 2010.

815 Sun, Y. L., Zhang, Q., Schwab, J. J., Chen, W. N., Bae, M. S., Lin, Y. C., Hung, H. M., and
816 Demerjian, K. L.: A case study of aerosol processing and evolution in summer in New York
817 City, Atmos Chem Phys, 11, 12737-12750, DOI 10.5194/acp-11-12737-2011, 2011.

818 Sun, Y.L., Zhang, Q., Schwab, J.J., Yang, T., Ng, N.L., Demerjian, K.L.: Factor analysis of
819 combined organic and inorganic aerosol mass spectra from high resolution aerosol mass
820 spectrometer measurements, Atmos. Chem. Phys., 12, 8537-8551, 2012.

821 Takami, A., Miyoshi, T., Shimono, A., Kaneyasu, N., Kato, S., Kajii, Y., and Hatakeyama, S.:
822 Transport of anthropogenic aerosols from Asia and subsequent chemical transformation, J
823 Geophys Res-Atmos, 112, Artn D22s31, Doi 10.1029/2006jd008120, 2007.

824 Takegawa, N., Miyakawa, T., Kondo, Y., Jimenez, J. L., Zhang, Q., Worsnop, D. R., and
825 Fukuda, M.: Seasonal and diurnal variations of submicron organic aerosol in Tokyo
826 observed using the Aerodyne aerosol mass spectrometer, J Geophys Res-Atmos, 111, Artn
827 D11206, Doi 10.1029/2005jd006515, 2006.

828 Timonene, H., Karjalainen, P., Asukko, E., Saarikoski, S., Aakko-Saksa, P., Simonen, P.,
829 Murtonen, T., Maso, M.D., Kuuluvainen, H., Bloss, M., Ahlberg, E., Svenningsson, B., Pagels,
830 J., Brune, W.H., Keskinen, J., Worsnop, D.R., Hillamo, R., Rönkkö, T.: Influence of fuel ethanol
831 content on primary emissions and secondary aerosol formation potential for a modern
832 flex-fuel gasoline vehicle, Atmos. Chem. Phys., 17, 5311-5329, 2017.

833 Tröstl, J., Chuang, W.K., Gordon, H., Heinritzi, M., Yan, C., Moltini, U., Ahlm, L., Frege, C.,

834 Bianchi, F., Wagner, R., Simon, M., Lehtipalo, K., Willaimson, C., Craven, J.S., Duplissy, J.,
835 Adamov, A., Almeida, J., Bernhammer, A.-K., Breitenlechner, M., Brilke, S., Dias, A., Ehrhart,
836 S., Flagan, R., Franchin, A., Fuchs, C., Guida, R., Gysel, M., Hansel, A., Hoyle, C.R., Jokinen, T.,
837 Junninen, H., Kangasluoma, J., Keskinen, H., Kim, J., Krapf, M., Küsten, A., Laaksonen, A.,
838 Lawler, M., Keiminger, M., Mathot, S., Möhler, O., Nieminen, T., Onnela, A., Petäjä, T., Piel,
839 F.M., Miettinen, P., Rissanen, M.P., Rondo, L., Sarnela, M., Schobesberger, S., Sengupta, K.,
840 Sipilä, M., Smith, J.N., Steiner, G., Tomè, A., Virtanen, A., Wagner, A.C., Weingartner, E.,
841 Wimmer, D., Winkler, P., Ye, P., Carslaw, K.S., Curtius, J., Dommen, J., Kirkby, J., Kulmala, M.,
842 Riipinen, I., Worsnop, D.R., Donahue, N.M., Baltensperger, U.: The role of low-volatility
843 organic compounds in initial particle growth in the atmosphere, Nature, 533, 527-531,
844 2016

845 Wang, Y. Q., Zhang, X. Y., and Draxler, R. R.,: TrajStat: GIS-based software that uses various
846 trajectory statistical analysis methods to identify potential sources from long-term air
847 pollution measurement data, Environ. Modell. Softw. 24, 938-939, 2009.

848 Wu, Z. J., Cheng, Y. F., Hu, M., Wehner, B., Sugimoto, N., and Wiedensohler, A.: Dust events
849 in Beijing, China (2004–2006): comparison of ground-based measurements with columnar
850 integrated observations, Atmos. Chem. Phys., 9, 6915-6932, 10.5194/acp-9-6915-2009,
851 2009.

852 Zhang, J., Wang, Y., Huang, X., Liu, Z., Ji, D., Sun, Y.: Characterization of organic aerosols in
853 Beijing using an aerodyne high-resolution aerosol mass spectrometer, Adv. Atmos. Sci.,
854 32(6), 877-888, 2015.

855 Zhu, Q., Huang, X.-F., Cao, L.-M., Wei, L.-T., Zhang, B., He, L.-Y., Elser, M., Canonaco, R.,
856 Slowik, J.G., Bozzetti, C., El-Haddad, I., Prévôt.: Improved source apportionment of organic
857 aerosols in complex urban air pollution using the multilinear engine (ME-2), Atmos. Meas.
858 Tech., 11, 1049-1060, 2018.

859

860

861

Acknowledgement

This research was supported by Basic Science Research Program through the National Research Foundation of Korea (NRF) funded by the Ministry of Science, Information, and Communications Technology & Future Planning (NRF-2017R1A2B4012143). E. Kang specially thanks for the support from the Basic Science Research Program through the National Research Foundation of Korea (NRF) funded by the Ministry of Education (NRF-2011-355-c00174).